International Journal of Concrete Structures and Materials

RESEARCH

Open Access

Sustainable Polyurethane-Based Polymer Concrete: Mechanical and Non-destructive Properties with Machine Learning Technique

S. I. Haruna[1,2*], Han Zhu[2,3], Yasser E. Ibrahim[1], Jian Yang[2], AIB Farouk[4], Jianwen Shao[5], Musa Adamu[1] and Omar Shabbir Ahmed[1]

Abstract

Polyurethane-based polymer concrete (PUC) has become a popular material for pavement repair. However, its compressive strength (f_c) is essential to achieve effective repair work. This study predicted the compressive strength and evaluated the non-destructive test (NDT) properties of the PUC mixtures, prepared by mixing aggregate-to-polyurethane (PU) at 80/20, 85/15, and 90/10 ratios by weight. The experimental datasets from mechanical and NDT tests were utilized to train machine learning (ML) models, including multilinear regression (MLR), artificial neural network (ANN), support vector machine (SVM), Gaussian regression process (GPR), and stepwise regression (SWR) models for estimating the f_c. Moreover, scanning electron microscopy (SEM) was employed to evaluate the microstructure of PUC. Feature selection tools were used to explore optimal input variables for estimating the (f_c) of the PUC samples. The PUC-10 specimen revealed a maximum ultrasonic pulse velocity (UPV) value of 3.05 km/h. The microstructure analysis shows micro-voids with crack propagation between the aggregate and PU binder in the specimen containing 10% PU after testing. All the developed models showed high prediction accuracy. In addition, SVM outperformed other models at the training phase with R^2 values of 0.9614, and ANN demonstrated the highest performance at the testing phase with R^2 values of 0.9502.

Keywords Machine learning, Polyurethane, Polymer concrete, Repair, Compressive strength, Pavement

1 Introduction

Concrete/flexible pavements are often prone to distress, such as rutting, aging, potholes, and cracks, during their life cycle due to environmental factors, including high temperature, impact, blast loads, chemical attacks, and moisture movement. However, conventional polymer modifiers can improve asphalt performance to a certain level; their stability under storage and aging resistance remains an issue (Cong et al., 2019; Ibrahim Haruna et al., 2021; Jiang et al., 2022a). PU is commonly used in asphalt pavement as modified asphalt and a repair material. It is formed by reacting polyols (including diols) with polyisocyanate (including diisocyanate). The block structure of PU is similar to that of styrene-butadiene rubber. Isocyanates and chain extenders produce a hard segment, while polyols have a soft segment (Li & Liu, 2002). Polyurethane demonstrated good mechanical behavior, corrosion resistance, high elasticity, durability, fatigue, impact resistance, and fast setting, responsible for its broad applications including adhesive, thermoplastic, and

*Correspondence:
S. I. Haruna
sharuna@psu.edu.sa
[1] Engineering Management Department, College of Engineering, Prince Sultan University, 11586 Riyadh, Saudi Arabia
[2] School of Civil Engineering, Tianjin University, Tianjin 300350, China
[3] Key Laboratory of Coast Civil Structure Safety of the Ministry of Education, Tianjin University, Tianjin 300350, China
[4] Interdisciplinary Research Center for Construction and Building Materials, King Fahd University of Petroleum and Minerals, 31261 Dhahran, Saudi Arabia
[5] School of Civil Engineering, Ludong University, Yantai 264025, China

several industries (Al-Atroush et al., 2021; Junaedi et al., 2023; Wang et al., 2021). Carrera et al. (2015) revealed that the asphalt mixture containing PU experienced several degrees of modification in the asphalt matrix structure and investigated the possible way to formulate the modified asphalt emulsion with polyether polyurethane. Meng et al. (2021) suggested that PU-modified asphalt is suitable for paving bridge decks. Moreover, different PU types have been used as modified asphalt, such as thermoplastic PU (Gallu et al., 2020) and MDI-polypropylene glycol prepolymer (Sun et al., 2018). In addition, the mechanical and impact resistance properties of PUC were studied. For instance, Huang et al. (2020a) investigated the hardened properties of PUC incorporated with ground glass fiber as pavement repair materials. Vasconcelos et al. (2005) reported that the incorporation of milled fiber in the PUC improves the wearing and dynamic properties. Jung et al. (2014) investigated the serviceability of PUC as repair materials for the runway. The author studied the mechanical properties, real-time degree of curing, and thermal expansion of the PUC specimen.

Over the decades, traditional linear and nonlinear methods have been utilized to estimate concrete properties. However, these methods have shortcomings in evaluating complex problems. Artificial intelligence-based models are applied to offer solutions to several engineering problems. These include GPR (Hoang et al., 2016), SVR (Chen et al., 2022), emotional intelligence, and a traditional feedforward neural network (FFNN) (Haruna et al., 2021), deep neural decision forest (Alrayes et al., 2023), Hammerstein–Wiener and SVM model (Adamu et al., 2021), ANN, regression tree, and random forest (Ehsani et al., 2022) that are adopted. Kooshkaki et al. (2019) developed an ANN to study the influence of porosity on estimating the hardening behavior of cement mortar modified with nanomaterials. Recently, advanced and complex machine learning techniques, capable of handling linear and nonlinear datasets, have attracted the attention of several researchers to predict and optimize concrete properties. For instance, Gad et al. (2024) developed automated machine learning (AML) to estimate the engineered geopolymer composite's compressive strength using the PyCaret library. The comprehensive datasets (132) of different mix design parameters from the experimental test conducted by the authors were utilized to train twenty (20) ML models. The result indicated that gradient boosting regressor (GBR) and CatBoost outperformed all other techniques in estimating the strength. Javid et al. (2024) forecasted the compressive strength of concrete containing silica fume using ensemble ML and gray wolf optimization techniques. The authors utilize a dual-objective optimization approach to study the difference between accurate forecasting and the simplicity of the models. The modeling task involves a 2995 dataset obtained from concrete specimens made from silica fume content of 5% to 30% by cement weight, collected from past studies. Song et al. (2021) developed ML models for estimating the compressive strength of concrete mixtures involving fly ash. Another study by Akber (2024) reported an improved forecasting of concrete strength related to model fitness and accuracy. The study involved a large dataset computing 26 input parameters based on mix proportions, engineered ratios, and environmental parameters. The compressive strength of self-compacting concrete involving recycled aggregate was predicted by Yang et al. (2024).

Similarly, previous studies have evaluated the mechanical properties of PU-based cement concrete (PPC) through AI-based models. Gao and Sun (2020) developed theoretical and experimental techniques to evaluate the PPC's fatigue life under varying temperatures. The authors reported that the proposed formula has successfully determined the PPC's fatigue life. Diaconescu et al. (2013) developed an ANN model to investigate the impact of epoxy resin composition and crumb rubber on the hardened behavior of PPC. Marinela et al. (2012) utilized an artificial neural network technique to estimate the strength of PPC modified with fly ash and resin content. However, to the best of the authors' knowledge, ML models have never been applied so far to forecast the mechanical behavior of the PUC.

2 Research Significance

Several studies have been carried out to evaluate the mechanical performance of PUC considering different parameters, particularly percentage PU binder composition (Huang et al., 2020b, 2021; Ibrahim Haruna et al., 2021; Jung et al., 2014; Wang et al., 2021) and some admixtures to modify its performance and effect on hardness segment (Cong et al., 2019, 2021; Huang et al., 2020a; Vasconcelos et al., 2005). While studying the effect of different PU content levels is beneficial, exceeding a certain PU binder content can lead to the development of more voids in the microstructure of PUC, resulting in strength loss; finding a trade-off involving optimum PU content that provides excellent performance is required to produce a sustainable PUC for pavement repair. This can be achieved by analyzing the results of the destructive and non-destructive tests and modeling.

In this respect, this work was conducted as the first study to predict compressive strength. PUC incorporated key input parameters related to material, non-destructive, and mechanical properties. The main aim of this study is to comprehensively forecast the compressive strength of PUC through linear and nonlinear regression models,

i.e., MLR, ANN, SVM, and GPR, based on the potential input parameters, including PU binder, density, flexural strength, ultrasonic pulse velocity, amplitude, and travel time for an ultrasonic signal transmitted through PUC specimen. Moreover, the PUC's microstructure was investigated using SEM.

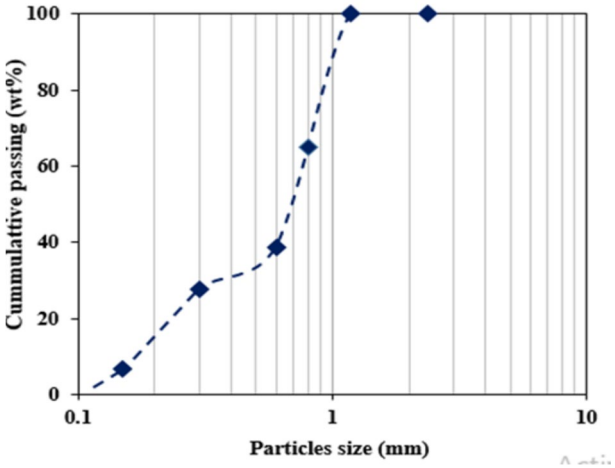

Fig. 1 Particle size distribution of the aggregate

3 Materials and Methods

3.1 Materials

3.1.1 Aggregate

The PUC mixtures were prepared using natural river sand, washed, air-dried, and sieved using a large sieve size of 2.26 mm; these fine aggregates were selected following Huang et al., (2020a, Ibrahim Haruna et al., (2021), and Jung et al., (2014). The aggregate has a particle size ranging from 0.3 to 2.26 mm with a fineness modulus and apparent density of 2.06 and 2650 kg/m^3, respectively. The distribution of particles of the aggregate is shown in Fig. 1.

3.1.2 PU Binder

The PU binders are produced through a polymerization reaction between polyol and isocyanates (Somarathna et al., 2018). The two components, namely polyol exhibiting hydroxyl group (–OH) and polymethylene polyphenylene isocyanate (PAPI), are used in this study, as presented in Fig. 2. Moreover, alkylene carbonate served as a diluent with a viscosity ranging from 5 to 15 CPS, a relative density of 1.18 g/cm^3, and boiling point of 220 °C which was introduced to the PU resin mixture to improve its performance (Jiang et al., 2021). The schematic process for the preparation of PU binder, bond mechanism,

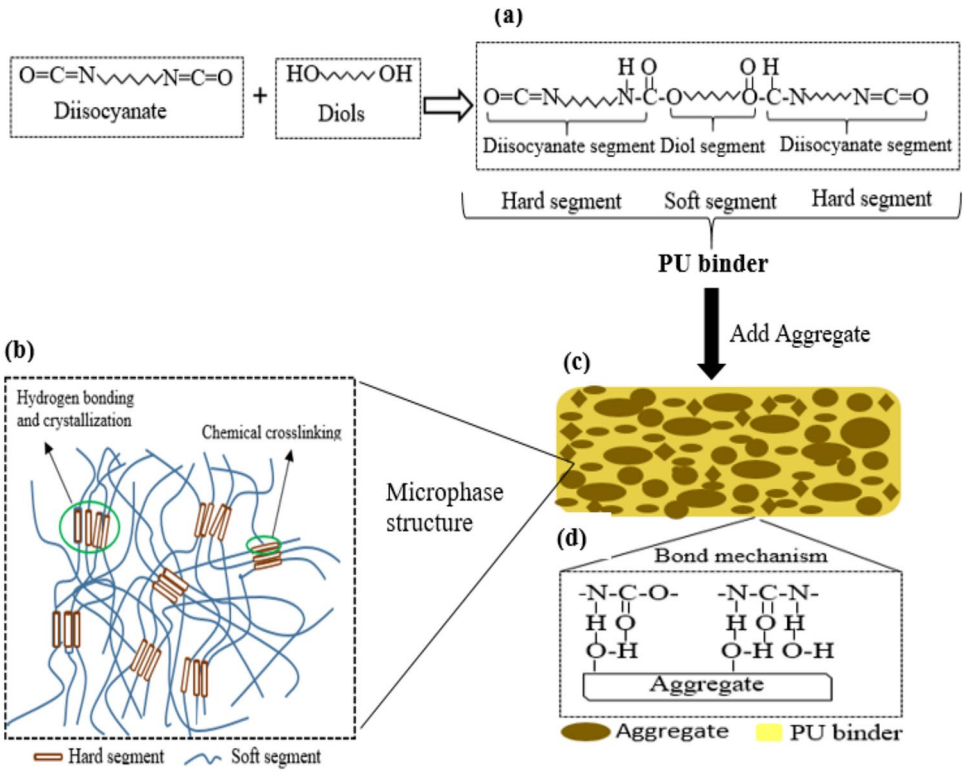

Fig. 2 Systematic procedure: **a** PU binder preparation, **b** molecular structure of PU, **c** PUC structure, and **d** bond structure between aggregate particle and PU material

Table 1 Technical indexes of PU resins

PU resin	Content/%	Viscosity (CPS at 25 °C)	Density (kg/m^3)
Polyol	70–90	35,000	1.5
PAPI	60–100	250	1.2
PU binder (Polyol:PAPI)			
Initial curing time		Final curing time	Flexural strength
3.5 h		72 h	5.50 MPa

Table 2 Formulation of PUC mixtures

Mixture ID	Aggregate:PU	PU binder		
		Polyol (g)	PAPI (g)	diluent (g)
PUC-20	80:20	167	33	8.35
PUC-15	85:15	167	33	8.35
PUC-10	90:10	167	33	8.35

and PU binder's microphase structure is shown in Fig. 2. The technical details of PU resin are listed in Table 1. In addition, the mixing ratio of 6:1 (polyol-to-PAPI) was adopted in this study. Figure 2d displays the bonding structure between the aggregate material and PU binder adhered by the powerful hydrogen bond contact close to the interface (Bistričić et al., 2010).

3.2 Preparation of the PUC

Three different mix ratios (aggregate-to-PU binder), including 80/20, 85/15, and 90/10, were adopted to prepare the PUC mixture. These mixing ratios adopted in this study were chosen following the past studies of Jung et al. (2014), Haruna et al., (2022), and Ibrahim Haruna et al., (2021). The formulation for manufacturing the PUC mixture containing PU binder (alternative hard and soft segments) is listed in Table 2. First, the PU matrix was made by combining the two components of PU resin in the presence of a diluent and mixing vigorously in a cup for 2 min to obtain a homogeneous mixture.

To prepare the PUC mixture, PU binder was mixed with aggregate vigorously, using a mechanical hand mixer for 2 min according to mixing ratios at room temperature placed in a container until a homogeneous mix was obtained, as depicted in Fig. 3. According to the mixing ratios, the fresh PUC mixtures were poured into the metallic mold. The samples were demoted after 5 h and kept at room temperature for 3 days.

3.3 Testing Procedure

3.3.1 Compression and Flexural Tests

The mechanical properties of PUC samples were tested following (DL/T5126-2001) (DL & T5126-, 2001, Test code on polymer-modified cement martor 2001) using a universal testing machine (UTM) (20-ton loading capacity), controlled at a speed rate of 0.2 mm/s for the flexural and compression test, respectively. The mechanical properties' test setup is shown in Fig. 4. The prismatic sample 40 × 40 × 160 mm^3 was used to measure the flexural strength of PUC samples. The samples were set up on two platforms with a 100 mm clear distance.

3.3.2 Ultrasonic Pulse Velocity Test

The homogeneity and quality of PUC samples at 3 days of curing age were assessed using the UPV test. The PUC specimen's strength and quality were determined by measuring the ultrasonic pulse velocity traveling through a cylindrical sample 100 mm × 75 mm (diameter × height) using NM4B non-metal ultrasonic equipment (Fig. 5). The sample was placed between a pair of ultrasonic transducers parallel to the PUC sample. Petroleum jelly was applied to the contact surface area between the test specimen and the transducers to ensure adequate pulse transmission. The signal was transmitted through the PUC, second transducer (received signal), and the travel time. The test was

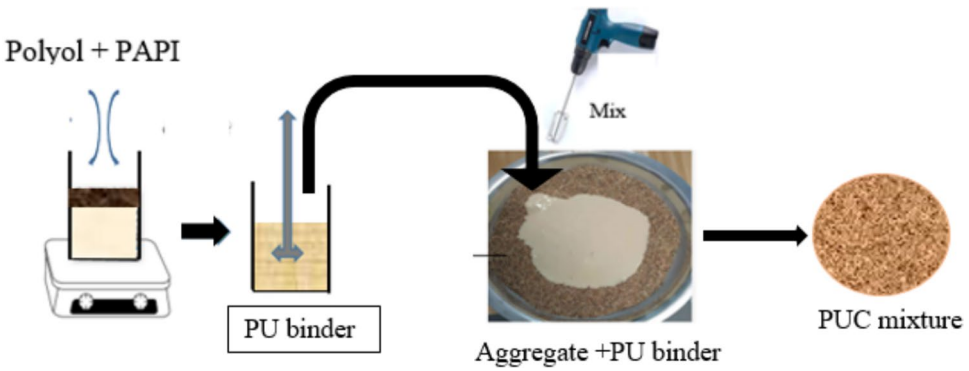

Fig. 3 Preparation of PUC mixture

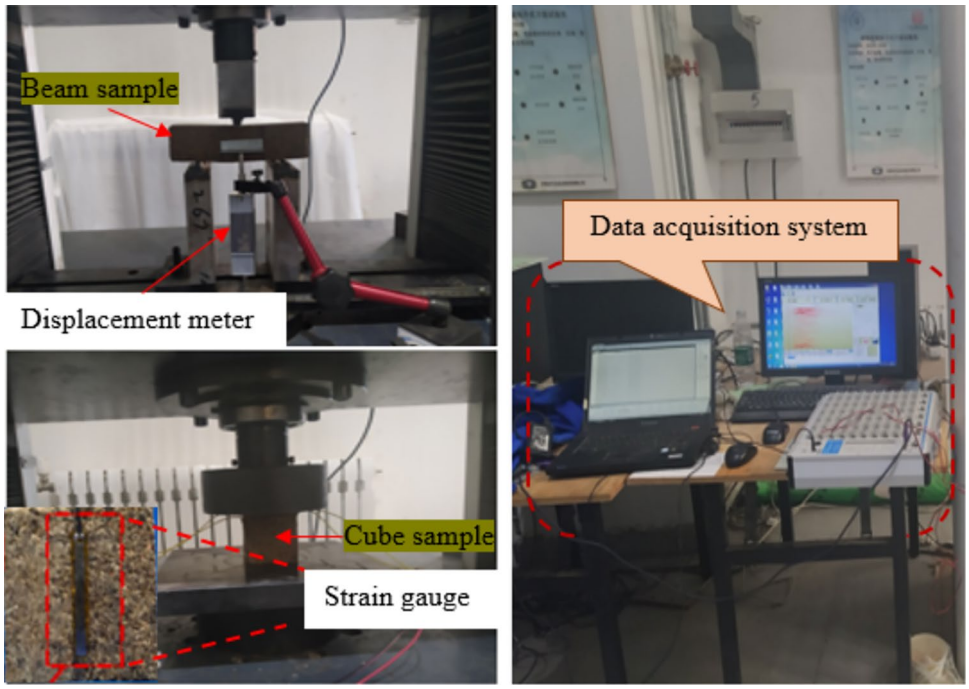

Fig. 4 Experimental setup for mechanical properties test

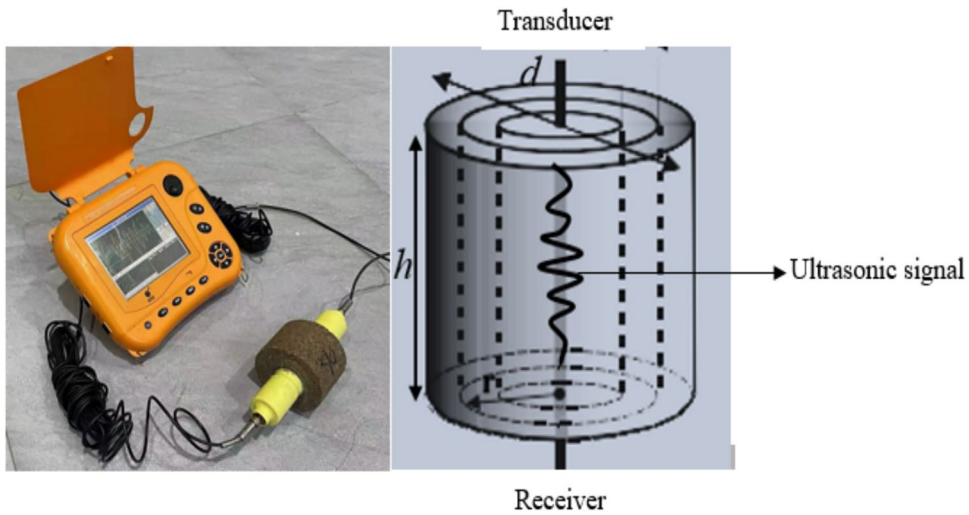

Fig. 5 Experimental setup for ultrasonic pulse velocity

repeated 12 times to achieve a reliable result. Therefore, Eq. (1) was used to determine UPV of the test samples:

$$V(h,t) = h/t \tag{1}$$

where $V(h, t)$ is the ultrasonic pulse velocity (km/h), h is the thickness of the specimen, and t is the travel time.

3.3.3 Microstructure Analysis

The microstructure of the PUC specimens was analyzed using an SEM test. The TESCAN MIRA4 was employed for the micromorphology observation of PUC at an accelerating voltage of 15 kV. After the compressive strength test, a PUC sample from each group

Table 3 Descriptive statistics of the dataset

Direction	Parameters	Symbols	Units	Mins	max	Mean	SD
Inputs	PU content	PU	%	10	20	15	4.09
	Density	ρ	kg/m3	1730.5	2200	1967	97.16
	Flexural strength	fy	MPA	3.9	11.68	1.76	3.09
	UPV	V	km/h	1.736	3.23	2.69	0.37
	Amplitude	A	dB	89.8	115.3	102.72	4.53
	Travel time	t	μs	23.2	43.2	28.52	4.73
Output	**Compressive strength**	**fc**	**MPa**	**11.1**	**33.66**	**21.75**	**6.37**

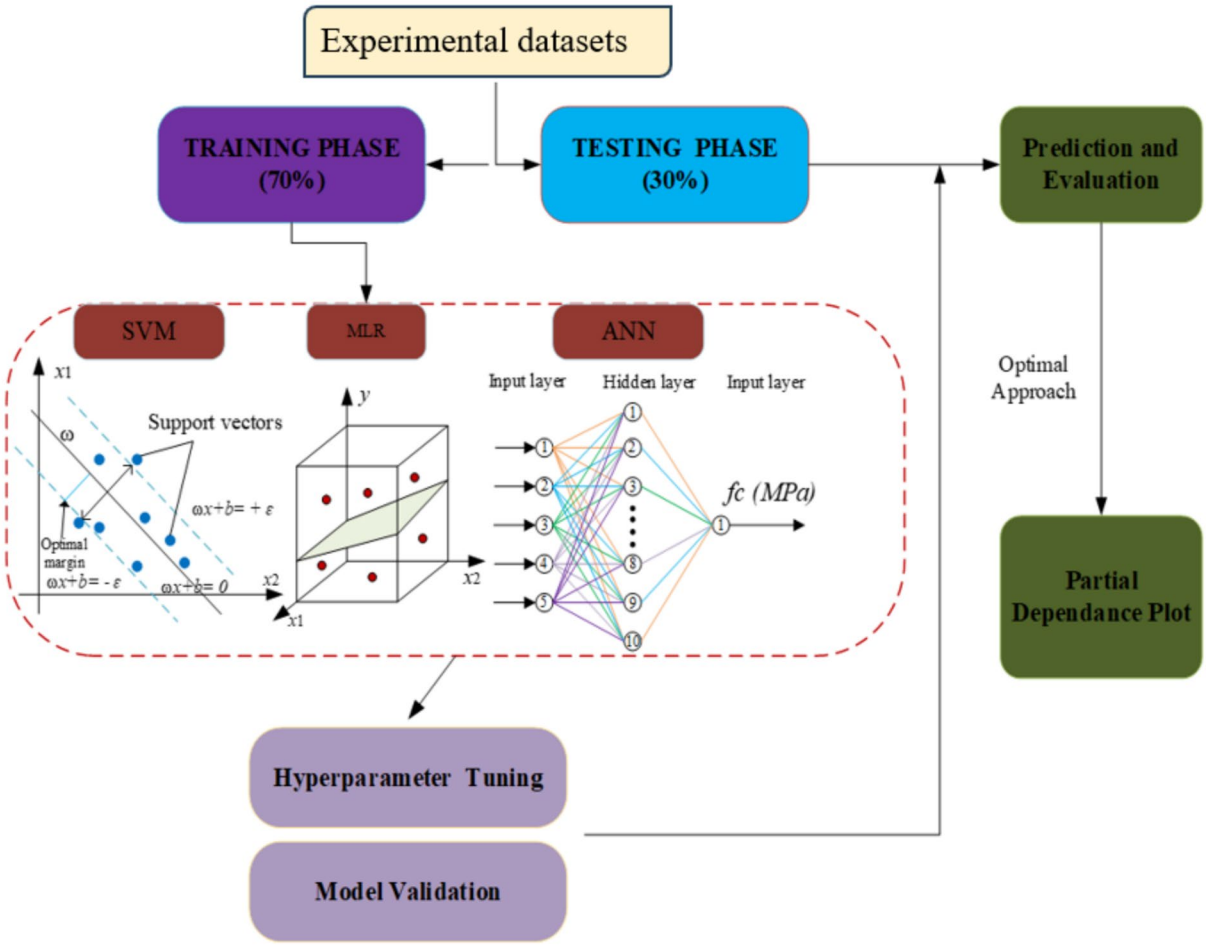

Fig. 6 Structure of ML models

was selected from the broken samples, cut into smaller pieces of 5 mm cubes, and used for the SEM test.

4 Machine Learning Algorithms

This study employed five (5) ML algorithms to train 150 experimental datasets to predict PUC's compressive strength. The dataset consists of seven (7) input variables based on the feature selection technique. The dataset was developed from the different experimental tests conducted in this study. The expressive statistic of the dataset is summarized in Table 3. The structure of ML models is depicted in Fig. 6.

4.1 MLR

MLR is a popular model used to establish the relationship between input $x, x \in Q^{n\times m}$ and output parameters labeled as $y, y \in Q^{n\times 1}$. Generally, multilinear regression can be illustrated mathematically, as in Eq. (2):

$$y = c_0x_0 + c_1x_1 + c_2x_2 \ldots c_nx_n = \sum_{i=1}^{n} c_ix_i = c^Tx \tag{2}$$

where c_0 c_1.... c_n are the model partial regression coefficient, and c_0 is the intercept at the y-axis with x_0=1. The solution of the multilinear regression technique is based on the least-squares approach, given in Eq. (3). The fitness of the model is accomplished by reducing the sum of the squares of the target and measured values Z:

$$Z = \left(y - Xc\right)^T \left(y - Xc\right) \tag{3}$$

4.2 ANN

ANN is a robust model for simulating a complex problem, which uses a dataset to establish a relationship between the output and input variables (Alas et al., 2020; Haruna et al., 2025a). The neural network consists of interrelated neurons at different levels, such as input, hidden, and output layers. The primary processing elements of an NN are referred to as nodes (Kumar et al., 2014). The inputs are reproduced by a changing weight to create the output for the neurons before being delivered to the transmission function, and the activation function combines the biased and weighted inputs. The two activation functions that are frequently used are those in Eqs. (4) and (5) are logistic and hyperbolic tangents:

$$f(x) = \left(\frac{1}{1+e^{-r}}\right) \tag{4}$$

$$f(x) = \left(\frac{e^{x} - e^{-x}}{e^{x} + e^{-x}}\right) \tag{5}$$

where $f(x)$ is the activation function.

4.3 GPR

The GPR refers to a reliable nonlinear prediction and supervised algorithm that simplifies the complicated and nonlinear function mapping hidden in datasets. In recent years, researchers from several scientific and engineering fields have become increasingly interested in GPR to solve problems (Omran et al., 2016). Due to the kernel functions, Gaussian process regression can handle nonlinear data. A Gaussian process regression model can also deliver an accurate response to input data, which is regarded as an advantage in modeling work (Pal & Deswal, 2010).

For a training set, $K = \left\{\left(z_i, y_i\right) | i = 1, \ldots n\right\}$. The input features $Z \in R^{K\times n}$ are referred to as the design matrix, and $y \in R^n$ *is* the output vector. The main theory of the GPR model is that the predicted parameter y is expressed as (Williams & Rasmussen, 2006)

$$y = f(z) + \varepsilon \tag{6}$$

where $\varepsilon \sim N(0, \sigma_n^2), \in R$ is the homoscedastic noise of all samples (z_i).

4.4 SVM

SVM was initially developed by Vapnik in 1995. It is a powerful and innovative supervised ML algorithm that provides conditions for solving several engineering problems. SVM model works on statistical theories and minimizes structural risk to achieve better generalization performance. Linear support and nonlinear support vector regression are common SVM types (Abba et al., 2020). For instance, a set of training points of a dataset $[(h_1, q_1 \ldots, (h_nq_n)]$ is given, where $h_1 \in R^n$ and $q_i \in R^1$ are the input and output variables. The linear SVM function $f(h)$ mapped the input vector h_i in Eq. (7):

$$y = f(h) = w\phi(h_i) + b \tag{7}$$

where ω is the support vector variable, b is the bias, and q is defined as the $\mathcal{E}$-insensitive loss function ($L_\mathcal{E}$) expressed in Eq. (8):

$$L_\varepsilon(q) = \left|q - f(h)\right|_\varepsilon = \begin{cases} 0 \text{ if } \left|q - f(h)\right| \le \varepsilon \\ \left|q - f(h)\right|_\varepsilon \text{ otherwise} \end{cases} \tag{8}$$

4.5 SWR

Regression analysis is a common method for describing the relationships between the output and input features. It is critical to obtain the best prediction set that yields high prediction accuracy concerning output parameters (Yasar et al., 2012). Stepwise regression is a strategy for selecting the best set of independent parameters by adding or eliminating variables that have the most significant impact on the sum of the remaining squares. Through re-evaluating the quality of newly passed variables following their partial sum of squares, the SWR undertook a systematic refinement of the variable or multiple variables. If a base rule to fit the models is not satisfied when the partial sum of squares of any formerly included features is used, the collected values are shifted to the removal state, and the features mentioned above are eliminated stepwise until each remaining feature agrees with the base rule (Yasar et al., 2012). The stepwise synopsis can be created by employing the many linear regressions, as expressed in Eq. (9)

$$y = c_0 + c_1x_1 + c_2x_2 + \ldots c_ix_i \tag{9}$$

The free parameters are involved in the expression, according to their effect on the output feature (y). To sustain the statistical significance of the input feature, numerous *t*-tests are conducted for each determined variable once each input feature is added to the expression (Wu et al., 2020).

4.6 Normalization

The experimental dataset of the PUC sample was normalized using Eq. (10). To remove redundancy and improve integrity before modeling, the data were transformed to a dataset with a similar scale. The normalization technique reduces the computational expense and enhances model performance (Haruna et al., 2021):

$$y_{\text{norm.}} = \frac{y - y_{\text{min.}}}{y_{\text{max.}} - y_{\text{min}}.} \tag{10}$$

where $y_{\text{norm.}}$ is the normalized value, and y,$y_{\text{min.}}$, and $y_{\text{max.}}$ are the measured, largest, and smallest values in the dataset, respectively.

4.7 Hyperparameter Tuning and Cross-validation

Hyperparameters controlled the procedure of the ML technique structure. It was thought to be the greatest technique to increase the estimation model accuracy. This study uses Random search (Fig. 7) to tune the ML model of hyperparameters (Farouk & Jinsong, 2022; Haruna et al., 2025b). Cross-validation and tenfold validation were used to handle the model. The dataset was proportioned into 70/30 for training and testing, respectively. Table 4 shows the tuning procedure applied to calculate the maximum hyperparameters of the ANN, SVM, and GPR models to predict PUC's compressive strength.

Table 4 Model hyperparameter for modeling the compressive strength of the PUC with their corresponding search space for fine-tuning

Model	Hyperparameter	f_c dataset
ANN	Hidden layer size*	(10, 10)
	Max_iter	1000
	Activation function	tanh
	Tolerance	0.001
SVM	Kernel function*	Gaussian
	Kernel scale	2.4000
	Regularization parameter C*	0.4202
	Epsilon	0.042
	Tolerance	0.001
GPR	Basis function	constant
	Sigma	0.0637
	Kernel function	Matern52
	Kernel scale	0.3353–5.1169

4.8 Performance Evaluation

To assess the ML algorithm's performance, this study used five performance evaluation markers. These matrices include the coefficient of determination, Pearson correlation coefficient, mean square error, root mean square error, and mean absolute error, as expressed in Eqs. (11) to (15). The m_i and p_i are the observed and predicted values, respectively; p is the number of predictors. $\overline{m}$ is the mean of the observed data, and n is the number of observations:

$$R^2 = \left[\frac{\sum_{i=1}^{n}(m_i - \overline{m})(p_i - \overline{p})}{\sum_{i=1}^{n}(m_i - \overline{m})^2 \sum_{i=1}^{n}(p_i - \overline{p})^2}\right]^2 \tag{11}$$

$$\text{MSE} = \frac{1}{n}\sum_{i=1}^{n}(m_i - \overline{m}_i)^2 \tag{12}$$

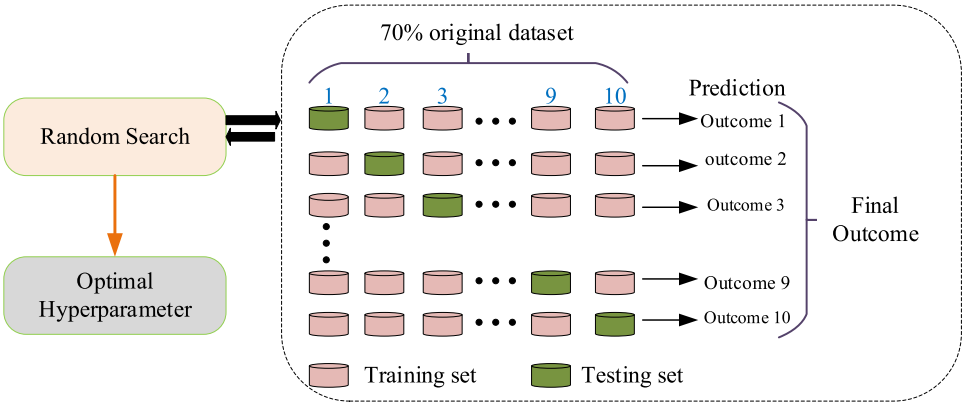

Fig. 7 Schematic illustration of the hyperparameter tuning process

$$R = \frac{\sum_{i=1}^{n}(m_i - \overline{m})(p_i - \overline{p})}{\sum_{i=1}^{n}(m_i - \overline{m})^2 \sum_{i=1}^{n}(p_i - \overline{p})^2} \quad (13)$$

$$\text{RMSE} = \sqrt{\frac{1}{n}\sum_{i=1}^{n}(m_i - p_i)^2} \quad (14)$$

$$\text{MAE} = \frac{1}{2}\sum_{i=1}^{n}|m_i - p_i| \quad (15)$$

5 Results and Discussion

5.1 Engineering Properties of PUC

The mechanical properties of the PUC samples are summarized in Table 5. These samples represent those of other PUC samples for modeling tasks. The PUC's average compressive and flexural strengths from each group were calculated at a 95% confidence level. The compressive strength of the PUC-20 is 31.07 ± 1.2, which is 40.65 and 98.53% higher than the samples containing 15 and 10% PU binder, respectively. The flexural strength of the PUC-20 was measured to be the peak strength of 10.47 ± 0.50 MPa, which is significantly higher than the samples containing 15 and 10% PU binder, respectively. The result agreed with the result obtained in the literature (Huang et al., 2020a; Jung et al., 2014). The mixture with the highest density revealed high strength, as shown in Table 5. The modulus of elasticity and failure strength increases with an increase in PU matrix content. The elastic modulus of the PUC-20 is 50.45 MPa, which is 102 and 125.4% higher than that of samples containing 10 and 15% PU binder, respectively. Upon reviewing the past study by Jung et al. (2014), utilizing epoxy resin to produce polymeric concrete indicated that the mechanical properties increase with epoxy content. PU binder content influences the mechanical properties and failure mechanism of the PUC specimens. Higher PU binder content led to the dense microstructure of the PUC, resulting in improved mechanical properties. This phenomenon was explained by microstructure analysis presented in Sect. 5.4, indicating that void and micro-crack

Table 5 Engineering properties of PUC

Mixing ratio	Code	Compressive strength (MPa)	Elastic modulus (MPa)	Failure strain (mm)	Density (kg/m^3)
Compression test					
PUC-20	1	32.46	63.51	1.08	2200
	2	30.89	41.51	1.06	2048
	3	29.87	46.32	1.22	2082
	Confidential level (95%)	31.07 ± 1.2	50.45 ± 10.68	1.12 ± 0.08	2076.67 ± 24.39
PUC-15	1	22.75	30.29	0.93	2048
	2	21.30	20.79	1.03	2032
	3	22.23	23.89	1.2	2051
	Confidential level (0.95)	22.09 ± 0.68	24.99 ± 4.47	1.05 ± 0.12	2059.7 ± 32.42
PUC-10	1	16.62	25.92	0.98	1939
	2	15.84	21.29	1.04	1989
	3	14.22	19.94	0.93	1936
	Confidential level (0.95)	15.65 ± 1.13	22.38 ± 2.89	0.98 ± 0.05	1954.7 ± 54.61
Mixing ratio	Code	Flexural strength (MPa)	Secant modulus (GPa)	Max. deflection (mm)	Density (kg/m^3)
Flexural (3-point bending) test					
PUC-20	1	10.47	1.98	0.74	2156
	2	9.93	2.28	0.61	2175
	3	11.02	2.62	0.60	2191
	Confidential level (0.95)	10.47 ± 0.50	2.29 ± 0.29	0.65 ± 0.07	2174 ± 16.18
PUC-15	1	6.86	1.35	0.77	2041
	2	6.42	0.98	0.91	2071
	3	6.65	0.97	0.81	2080
	Confidential level (0.95)	6.64 ± 0.26	1.1 ± 0.2	0.83 ± 0.06	2064 ± 31.68
PUC-10	1	5.01	0.36	3.09	1902
	2	4.17	0.47	1.58	1984
	3	5.33	0.21	4.45	1996
	Confidential level (0.95)	4.83 ± 0.55	0.35 ± 0.12	3.04 ± 1.32	1961 ± 47.26

propagation have disappeared due to the increasing PU binder content. However, a specific limit for PU binder content is required because very high PU binder content in the PUC mixture can lead to the propagation of more voids in the microstructure, thereby making the PUC specimen expand beyond its original shape, as reported in the literature (Jiang et al., 2022b). Due to the viscoelastic nature of PU binder, PUC specimens exhibit different failure mechanisms under ultimate load, which is influenced by PU binder content. The specimen with low PU binder content (PUC-10) exhibited brittle failure under flexural load, while the PUC specimen with high PU binder content showed elastic deformation before complete failure. Under compression load, all the specimens revealed crushing failure modes.

5.2 Ultrasonic Pulse Velocity

The homogeneity and quality of PUC samples were assessed using the UPV test. The ultrasonic wave velocity during the test depends on the material's density and elastic modulus. The high UPV value revealed good quality and homogeneity of the testing material, whereas the low pulse velocity revealed non-homogeneity (Ghosh et al., 2018).

Figure 8 shows the variation of UPV value among the three groups of PUC samples. The PUC-10 specimen exhibited the highest average UPV value of 3.05 km/h, which is higher by 22.53 and 20% compared to that of PUC-15 and PUC-20 specimens, respectively. The ultrasonic velocity through voids in the material is lower than that through the solid material. Therefore, in this study, PUC-10 specimens appeared to have more solid material, because of the high aggregate content, compared to the PUC-15 and PUC-20 specimens. Due to the presence of high fine aggregate materials consisting of silt material (0.3 mm particle size) and lesser PU binder content, the microstructure of the PUC-10 specimen is more homogeneous than the PUC-15 and PUC-20, and the homogeneity of the materials influences its UPV value. For this reason, PUC-10 demonstrated the highest UPV value. Although PUC-10 exhibits lower mechanical properties when compared to PUC-15 and PUC-20, it is clear that polymer concrete revealed low ultrasonic velocity compared to ordinary concrete as obtained in this study, and this finding agrees with the result obtained in the literature (Ghassemi & Toufigh, 2020; Ghosh et al., 2018). The UPV in ordinary concrete increases with increasing strength, which is attributed to material properties, mainly consisting of solid materials such as aggregate, sand, and cement interlocking each other, resulting in a dense concrete.

5.3 Relationship Between UPV and Compressive Strength

The possibility of adopting the ultrasonic techniques for the non-destructive evaluation of the hardening properties of PUC relies upon obtaining a sufficient regression function with a high correlation coefficient value near 1, considering the behavior of the PUC specimen concerning UPV. When a good relation is achieved between the UPV and any other parameter, such as compressive strength, flexural strength, density, and elastic modulus (Garbacz & Garboczi, 2003), the application of pulse velocity can be employed to evaluate PUC's mechanical properties of the PUC. This study evaluated the relationship (see Fig. 9) between the UPV and the compressive strength. The analysis result showed that the data point fitted the line using the linear regression function for the

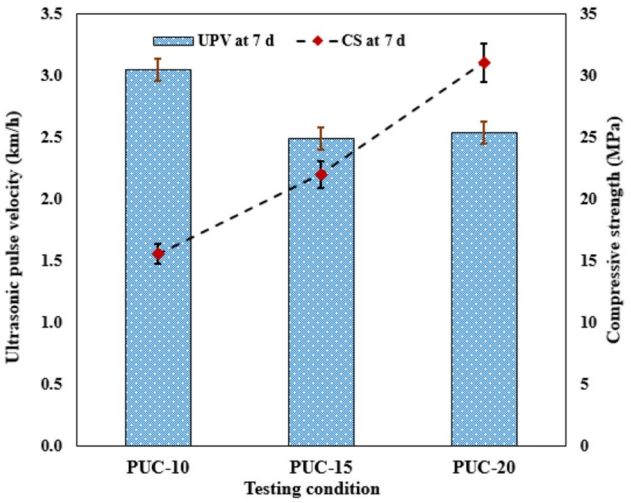

Fig. 8 Ultrasonic pulse velocity of PUC samples

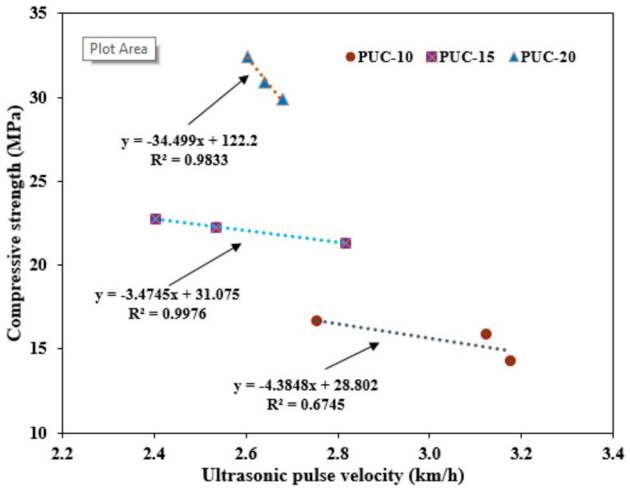

Fig. 9 Regression function between the UPV and compressive strength

compressive strength, and best fits were obtained from PUC-15 specimens with $R^2 = 0.9976$. The linear relationship between the UPV and compressive strength of PUC-10 and PUC-20 has a correlation factor of 0.6745 and 0.9833, respectively. The standard error in determining the compressive strength from the UPV was 0.4241–0.7532 MPa. This result indicated that the mechanical properties of PUC can be estimated using UPV with reasonable accuracy.

5.4 SEM Analysis of PUC

Figure 10 shows the SEM images of the microstructure of the PUC samples according to the mixing condition after compressive strength tests. These SEM images focus on the morphology of the interfacial adhesion between the aggregate and PU matrix to better understand their bonding performance. From Fig. 10a, b, the samples prepared with 10% PU binder (PUC-10) specimens showed the existence of micro-voids and the progression of cracks in the specimen's microstructure. This behavior is due to the low percentage of PU binder content used to prepare the sample. The microstructure showed that little PU binder had covered the aggregate surface; this finding agreed with Huang et al., (2020a) and Jung et al., (2014). Upon increasing the PU matrix content by 5%, a nearly dense structure (Fig. 10c, d) was achieved with nearly no micro-voids at the interface. However, craze-like structures appeared at the aggregate interface. This

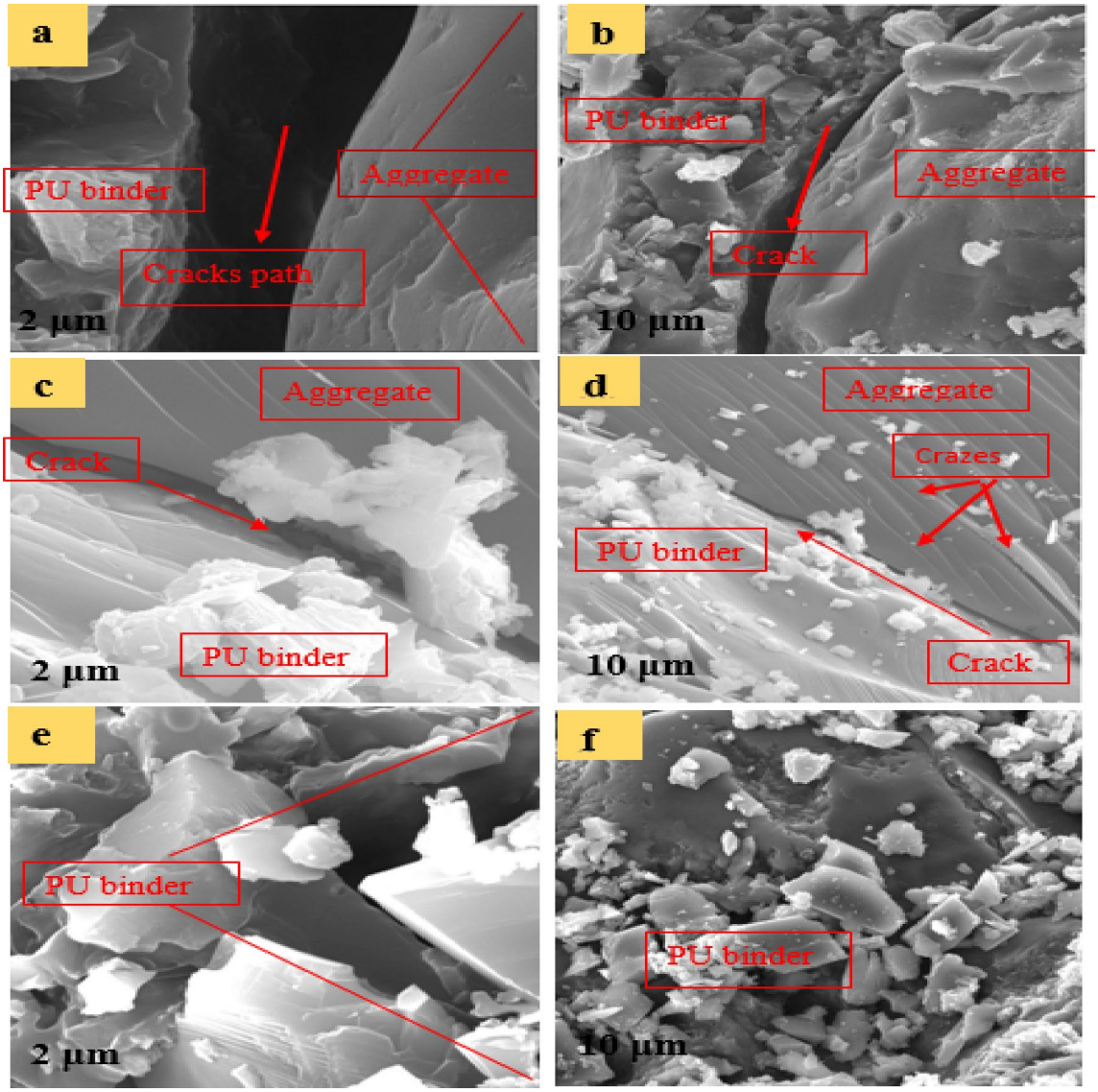

Fig. 10 SEM image of PUC after compressive strength test

phenomenon was explained by the viscoelastic behavior of PU composites, as found in the literature (Shao et al., 2020). The micro-void disappeared, and the width of the crack became narrow. The microstructure analysis of PUC-20 is depicted in Fig. 10e, f. Due to the high PU content, the SEM image displayed no visible cracks with a highly dense structure. The PU matrix in PUC-20 is sufficient to cover all the rough surfaces of the aggregate, suggesting a stronger bond strength leading to significantly improved PUC's mechanical properties.

5.5 Selection of Optimal Input Parameters

For any data-driven model to produce desired and reliable prediction results, an appropriate selection of relevant input variables is required. The feature section algorithm can be used to achieve the choice of input parameters. To decide the best input variables to model the PUC compressive strength, a sensitivity analysis utilizing Pearson correlation, mutual information, and minimum redundancy maximum relevance methods was applied. The nature of the experimental dataset is described using a distribution plot, as shown in Fig. 11. Some of the input variables follow a normal distribution, as in the case of density and amplitude depicted in Fig. 11b, e. The flexural and compressive strength datasets barely follow the normal distribution (Fig. 11c, g). Conversely, PU content, ultrasonic velocity, and travel distance do not follow the normal distribution; hence, most data are located away from the mean value in the superimposed normal curve, as shown in Fig. 11a, d, and f.

5.5.1 Sensitivity Analysis

Sensitivity analysis datasets have been widely used in research to handle inappropriate input parameters in the modeling work. Involving an unnecessary parameter reduces prediction accuracy and increases processing demand in an artificial intelligence model (Nourani & Sharghi, 2020). As shown in Fig. 12, the PC matrix was used to investigate the experimental dataset's most influential parameters. As a parameter approaches zero and closer to −1 or +1, its importance decreases. The positive value signified a direct relation and vice versa between the measured and predicted feature. As shown in Fig. 12, flexural strength and PU content were revealed to be the most sensitive parameters with a value of +0.9548 and +0.9102, respectively. In contrast, the ultrasonic pulse velocity indexes are inversely related to the target parameter, except for travel time.

5.5.2 Minimum Redundancy Maximum Relevance (mRMR)

The mRMR, developed by Peng et al. (2005), is regarded as one of the most powerful filter algorithms. It has been used to rank input feature sets according to their significance to the predicted parameter while penalizing input variable redundancy. The primary goal of mRMR is to establish the mutual information-based maximum dependency between the input feature X and the target feature P. The maximum relevance work is based on searching features that fulfilled Eqs. (16) to (18):

$$\max D(X,p); D = \frac{1}{|x|}\sum_{z_i \in X} I(X_i;p) \tag{16}$$

According to Peng et al. (2005), a minimal redundancy criterion is necessary since the greatest relevance condition can result in large redundancy when selecting potential input parameters:

$$\min R(X,p); R = \frac{1}{|x|}\sum_{x_i,x_j \in X} I\left(x_i,x_j\right) \tag{17}$$

The mRMR was produced by linking the D and R criteria in Eqs. (16) and (17) and optimizes the outcomes. The greedy algorithm could also be applied in real situations, where S is the set of selected input parameters:

$$\max_{X_i \notin s}\left[I(X_i;p) - \frac{1}{|S|}\sum_{X_j \in s} I\left(X_j;X_i\right)\right] \tag{18}$$

Figure 13 shows the result of feature selection to determine the optimal input parameter based on the mRMR method. The mRMR uses the predictor score to rank the parameters. As shown in Fig. 13, flexural strength is ranked first and has the highest importance score. The ultrasonic pulse velocity index (travel time) had the lowest importance score. On the other hand, amplitude appeared to be irrelevant to the compressive strength prediction of PUC concrete.

5.5.3 Mutual Information

The MI approach establishes statistical dependence between two measured features. The zero MI value denotes the absence of any statistical dependence between the two parameters. The dependency increases as the distance from zero increases (Umar et al., 2021):

$$\mathrm{MI}\left(x,y\right) = f\left(x\right) + f\left(y\right) - f\left(x,y\right) \tag{19}$$

where f(x) is the entropy function of x, and the joint entropy between the two features x and y is represented by f(x, y) and can be expressed in Eq. (17):

$$f\left(x,y\right) = -\sum x \in X \sum y \in Y . P_{XY}\left(x,y\right) \log P_{XY}\left(x,y\right) \tag{20}$$

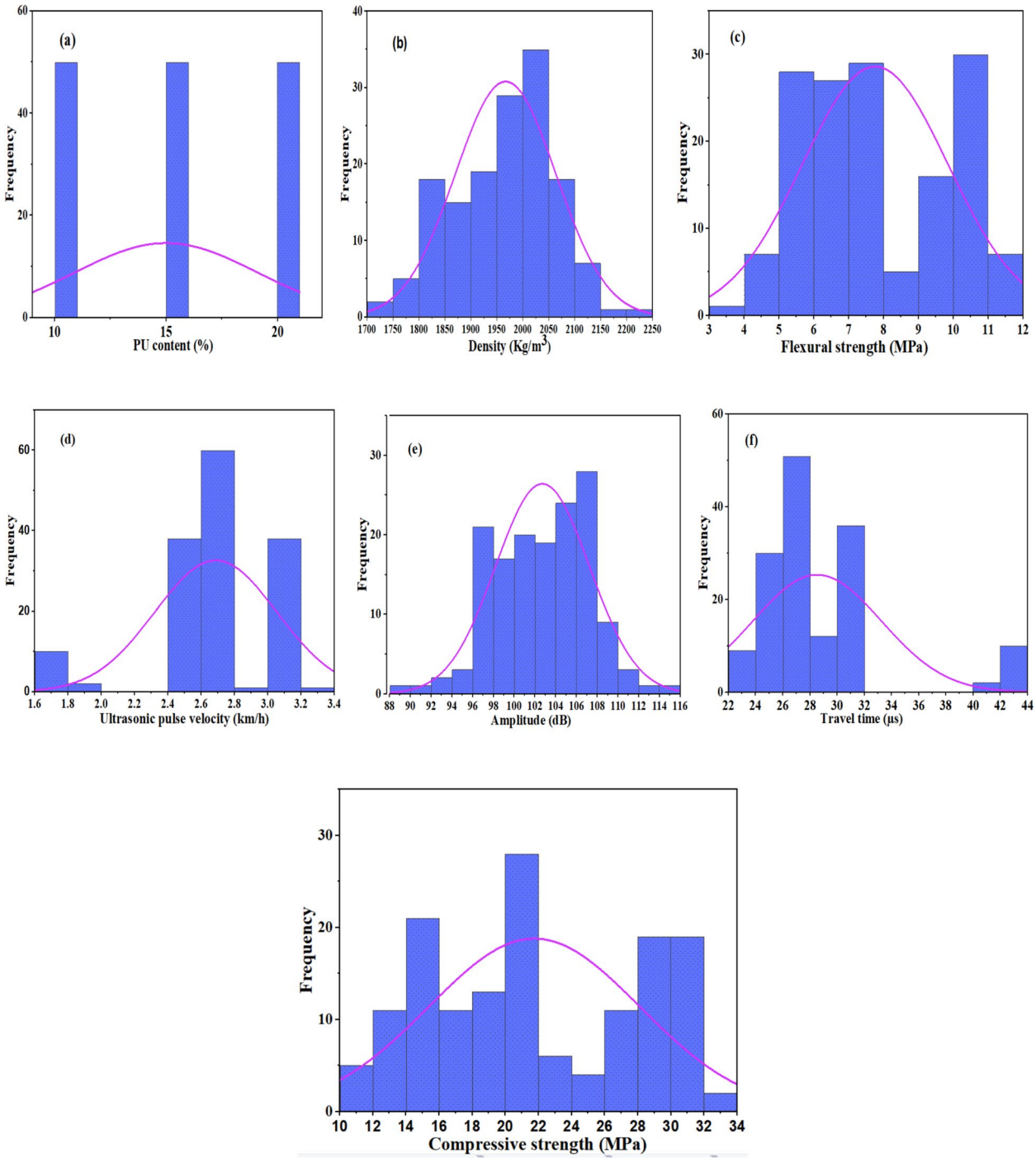

Fig. 11 The frequency distribution plots of the experimental datasets

Figure 14 demonstrates the dependence of each input parameter using the mutual information method. Therefore, the higher relevance input parameter is obtained with the MI value being higher than 0. As shown in Fig. 14, density, flexural strength, and amplitude turned out to be the most relevant variables based on the mutual information, with values of 1.6421, 1.4984, and 1.6443, respectively. This is attributed to the less scattered result obtained in these input parameters, which is normally distributed (Fig. 11b, c, and e). The least relevant

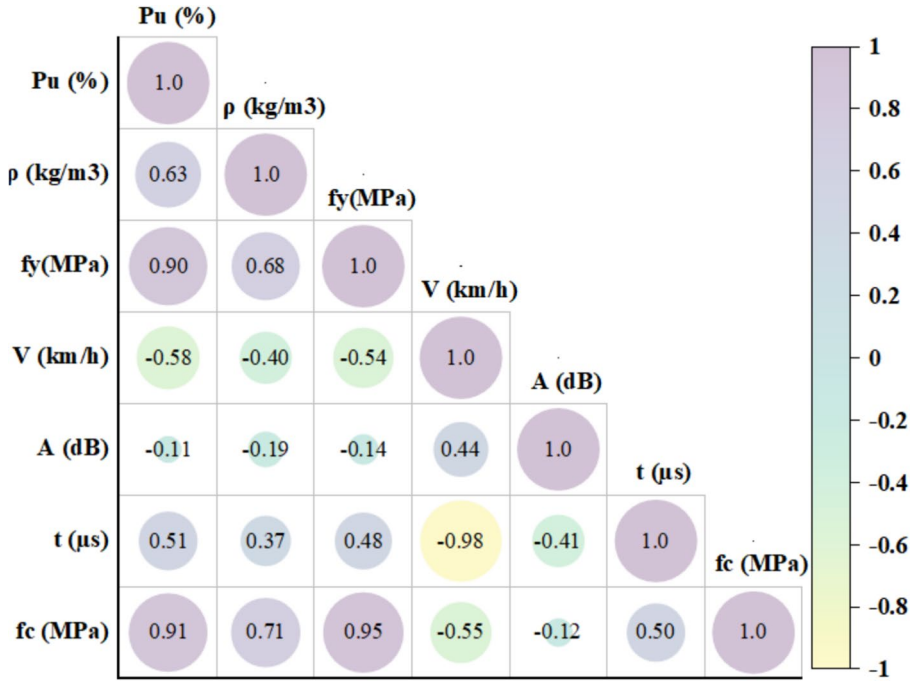

Fig. 12 Pearson correlation matrix

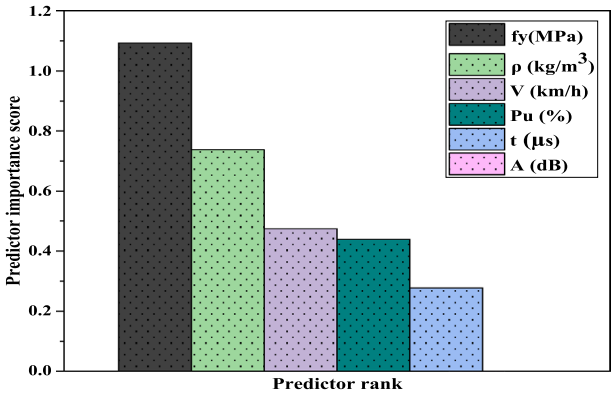

Fig. 13 Selection of optimal input parameters using mRMR techniques

parameter was PU content, with an MI value of 0.4202; this parameter is not normally distributed. Based on the result obtained in mutual information computation, it can be concluded that selecting potential parameters in terms of mutual information largely depends on the dataset's scatter.

The feature selection result indicated that travel time appeared to have a low relevance in modeling the compressive strength of PUC. However, mRMR showed that amplitude is a redundant parameter among the input parameters and is inversely related to the output parameter, as indicated in the Pearson correlation analysis. According to the results obtained from feature selection approaches; thus, it is essential to utilize linear and nonlinear approaches to select optimal input variables. Artificial intelligence models can involve linear and nonlinear relations parameters with the output parameters. All the parameters are significant, according to the outcome of the *t*-test between compressive strength and input variables.

6 Result of ML Algorithms

The model development was performed using MATLAB (2021a), and the model validation was executed utilizing a tenfold cross-validation approach (Farouk & Jinsong, 2022; Ibrahim Haruna et al., 2021). The datasets obtained experimental program include polyurethane content, density, flexural strength, ultrasonic pulse velocity, amplitude, and travel time, which were used as input parameters for the development of the ML model to predict the compressive strength of the PUC. Table 6 summarizes the results of the evaluation matrices of the ML models at the training and testing stages. As summarized in Table 6, the MSE, RMSE, MAE, and *R* measure the variation between the experimental and target values. Low MSE, RMSE, and MAE values translate to high estimation skills, and high R^2 and *R* values reveal high prediction skills. As presented in Table 6, all the developed ML algorithms predicted compressive strength with high accuracy at

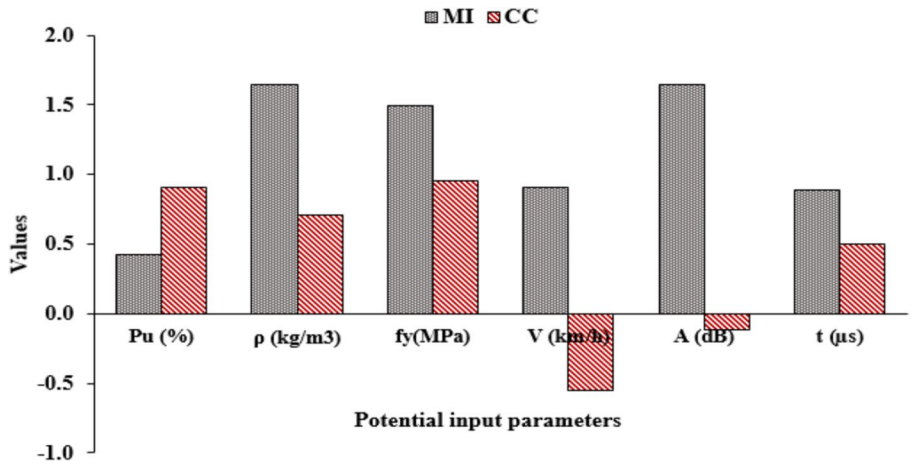

Fig. 14 Relevancy of input features using the MI method

Table 6 Evaluation metrics results for the different models

Models	Training					Testing				
	MSE	RMSE	R^2	R	MAE	MSE	RMSE	R^2	R	MAE
ANN	0.0037	0.0879	0.9566	0.9780	0.0493	0.0043	0.0811	0.9502	0.9748	0.0502
MLR	0.0055	0.0591	0.9324	0.9656	0.0566	0.0045	0.0584	0.9396	0.9693	0.0503
SVM	0.0031	0.1352	0.9614	0.9805	0.0441	0.0048	0.2842	0.9345	0.9667	0.0540
GPR	0.0032	0.0004	0.9606	0.9801	0.0434	0.0038	0.0458	0.9482	0.9738	0.0481
SWR	0.0047	0.0903	0.9424	0.9707	0.0518	0.0049	0.33072	0.9360	0.9675	0.0522

the modeling stages, with an R^2 value higher than 90%. In addition, SVM turned out to be the best model, based on the training value of $R^2 = 0.9614$, MSE = 0.0031 MPa, RMSE = 0.1352 MPa, and MAE = 0.0441 MPa. Generally, the evaluation matrices presented in Table 6 revealed insignificant differences among the developed ML algorithms. These selected ML algorithms have nearly equal performance for forecasting PUC's compressive strength. The result from the ML models showed that the number of samples and input parameters considered for the training is adequate without an overfitting problem.

The scatter plots between the measured and predicted values in the training stage are shown in Fig. 15. The data point was concentrated along the fitted line, indicating the higher goodness of fit of the ML models. The accuracy of the ML models was checked by determining R^2 values of the models at the modeling stages, as shown in Figs. 15 and 16. All the machine learning algorithms predicted compressive strength with high accuracy. Conversely, the ANN model demonstrates higher performance with an R^2 value of 0.9502 at the testing phase than other models, as shown in Fig. 16a. Previous studies have also indicated variations in the robustness of the model, as found in Hoang et al., (2020) and Thakur et al., (2021). In addition, the difference in model performance between SVM and ANN during training and testing can be explained by the fact that SVM, which appeared to be best in training accuracy, is due to its robust optimization strategy, may not always generalize well if overfitting occurs. In contrast, with appropriate training and regularization, ANN can achieve better generalization and hence outperform in the testing data. This aligns with established theoretical insights and underscores the importance of model selection and tuning based on both training and testing behavior,

The relative error distribution was used to check the accuracy of each developed ML model at the training and testing stages with the aid of a Boxplot, as shown in Fig. 17. The SVM model (Fig. 17a) exhibited good accuracy in predicting the strength of PUC at the training stage. The first- and third-quartile values of −8.2 and 6.3% are found in the SVM model. In addition, the error distribution exhibited by all the ML models was reasonably low at the two modeling stages (Fig. 17a), indicating the estimation skills of the models in computing the compressive strength of PUC. GPR also revealed a lower relative error distribution of 8.4%, while MLR and

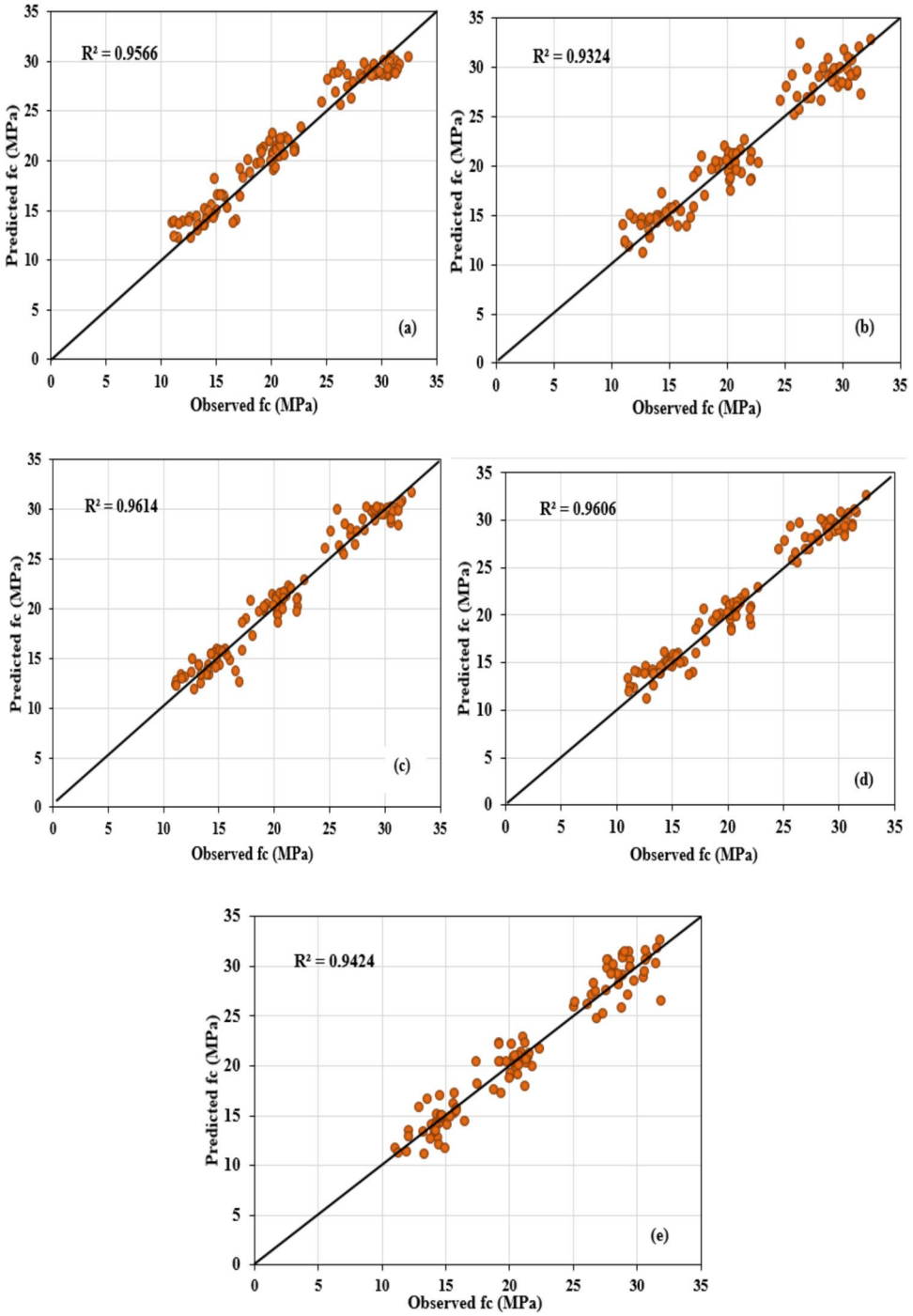

Fig. 15 Scatter plots between the experimental and predicted f_c values at the training stage for **a** ANN, **b** MLR, **c** SVM, **d** GPR, and **e** SWR models

ANN models have approximately equal relative error distributions.

Figure 17b shows lower error distribution in MLR, ANN, and SWR models during the training phase. Farouk and Jinsong, (2022) found a lower relative error distribution of MLR and ANN models among the ML models developed for estimating interface bond strength of UHPC-NSC. The minimum and maximum relative error distributions of −10.6 and 6.8% are obtained in ANN, respectively. The minimum and maximum relative error distributions of the MLR in the first and third quartiles are −8.7 and 6.7%, respectively. Generally, all

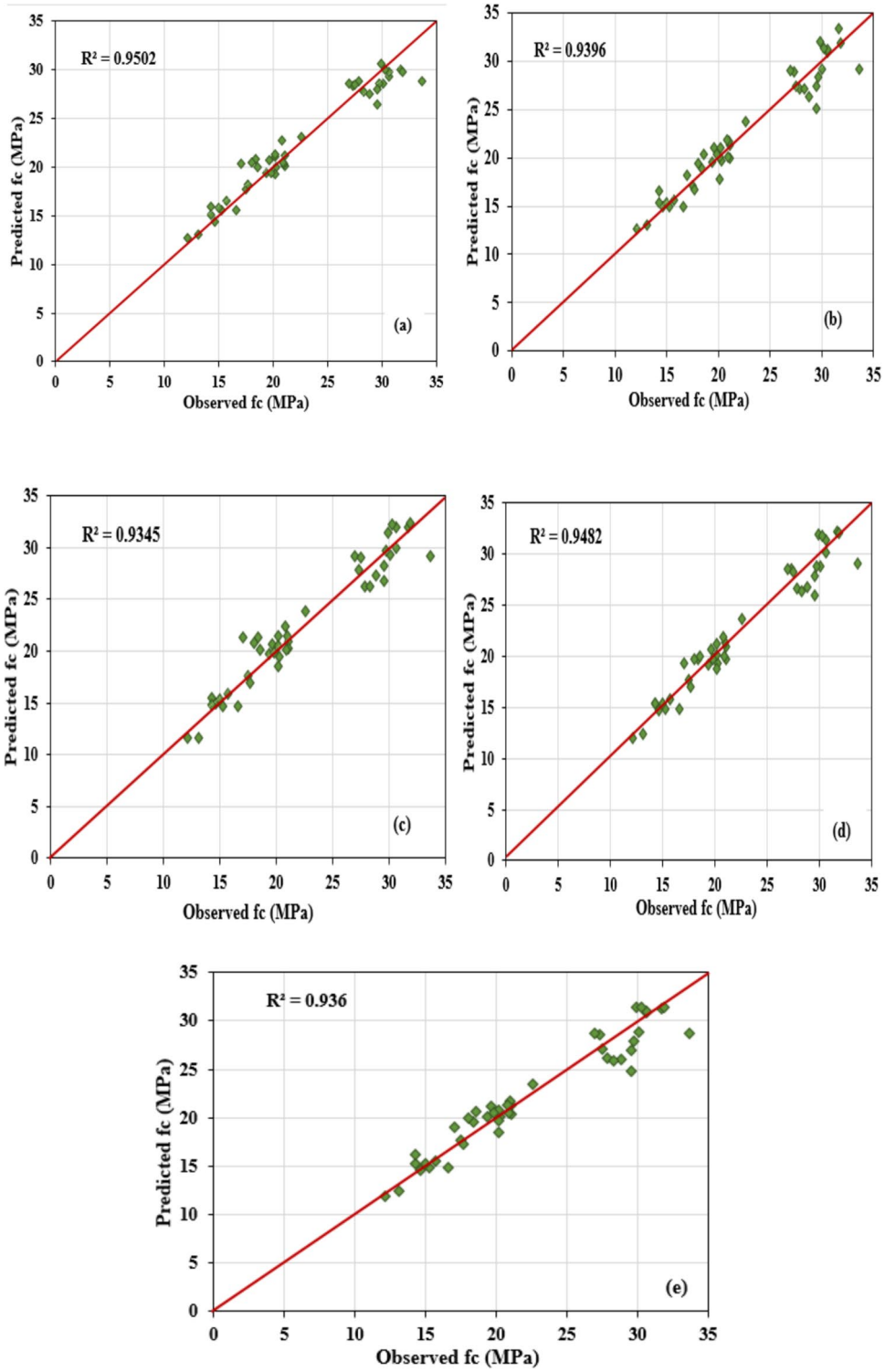

Fig. 16 Scatter plots between the experimental and predicted f_c values at the testing stage for **a** ANN, **b** MLR, **c** SVM, **d** GPR, and **e** SWR model

predicted the strength with a lower minimum and maximum relative error. This result was in agreement with the ANN model's good performance shown in a scatter plot during the testing phase compared to other models.

In addition, the Taylor diagram was used to compare model performance (Fig. 18a, b). The Taylor diagram is a comprehensive technique for comparing the model performance through three statistical indices,

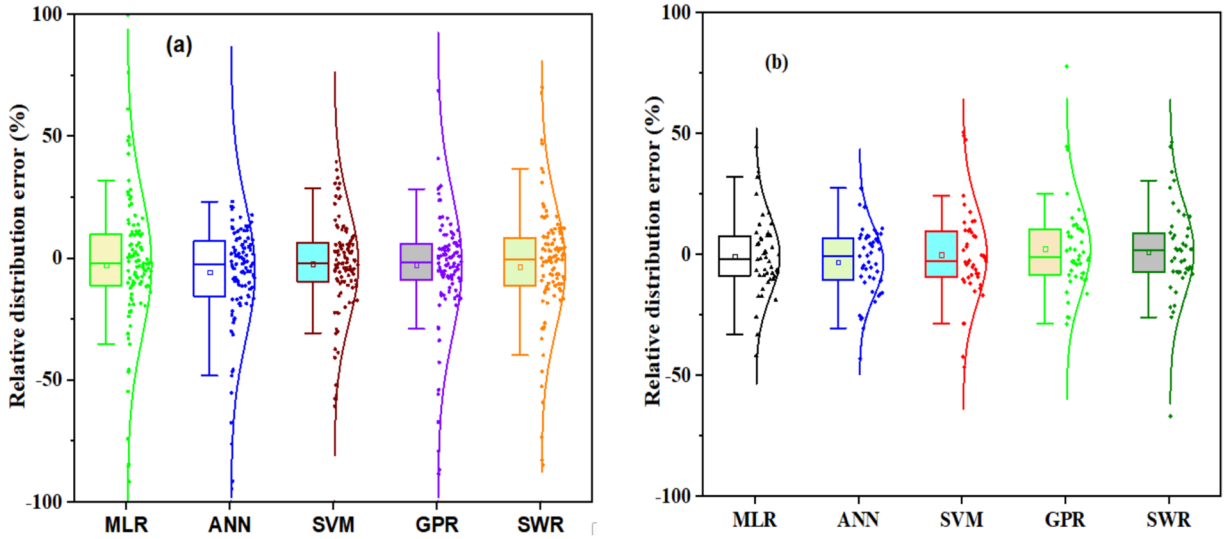

Fig. 17 Boxplot showing relative error distribution at **a** training and **b** testing stage

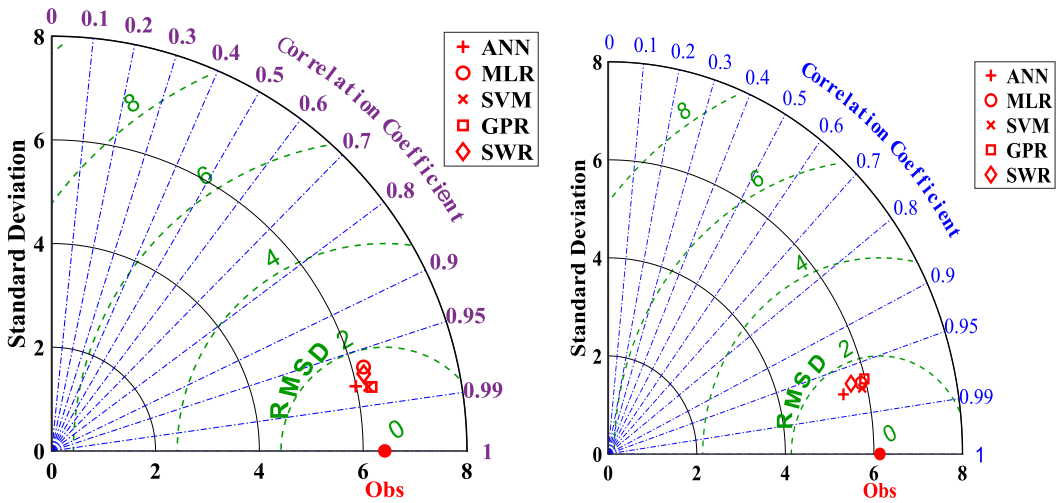

Fig. 18 Taylor diagram showing performance of the model at **a** training, **b** testing stage

including RMSE, R^2, and standard deviation. The relationship between the target and the experimental values is described by the azimuthal location. The RMSE is correlated with the point where the observed and predicted fields meet, and the relation increases with a decrease in RMSE. Thus, the radial point determined from the origin increases as the standard deviation trend increases (Taylor, 2001). The model is referred to as the best by point when $R^2 = 1$ (Yaseen et al., 2018).

From Fig. 18a, b, all the ML models demonstrate high performance in forecasting f_c with RMSE, correlation coefficient, and standard deviation closer to that of observed (Obs) data at two modeling phases. The SVM and ANN performed better than all other models concerning performance indicators. The developed ML models were clustered very closely, demonstrating the models' superior performance. The standard deviation of established models is lower than that of the observed data, explaining that the model's performance is not influenced by overprediction. However, error plots comparing model performance can be found in Long et al., (2023a) and Long et al., (2023b).

To further compare the performance of the developed ML models, a radar plot was employed to assess model performance (Fig. 19). The performance matrices were illustrated in the plots, revealing that some indicators have nearly equal matrices at the two modeling stages. However, some indicators revealed different values recorded at the training and testing stages, as indicated in Fig. 19c, e.

6.1 Characterization of the Effect of Input Variables on the Compressive Strength

6.1.1 Partial Dependence Plots for Input Variables

A partial dependence plot is used to interpret the black-box model for the best developed model that predicted the compressive strength in the overall dataset, which turned out to be the ANN model. The influence of each input variable can be determined primarily by how the pattern of the input variable affects the output (linear, monotonic, or complex). A partial dependence plot can view and analyze the interaction between the target and input parameters (Hastie et al., 2009). The effect of six input parameters from the experimental dataset for predicting PUC compressive strength was pictorially presented using partial dependence plots, as depicted in Fig. 20. Similar to the result obtained in feature selection of relevant variables, it can be seen from Fig. 20a that partial dependence plots identify the flexural strength as the optimal parameter that provides the highest prediction and distinct the influencing parameters. The interaction effects between the compressive strength and the input variables demonstrate a linear relationship except for PU content, as shown in Fig. 20b.

Moreover, the flexural strength, density, and travel time (Fig. 20a, c, and d, respectively) are directly proportional to the target response. At the same time, amplitude and velocity revealed an indirect relationship. This is similar to the result obtained in Sect. 4.2.1. The second and third optimal parameters are PU content and density, as indicated in partial dependence plots, and amplitude (see Fig. 20e) was found to be the least important parameter.

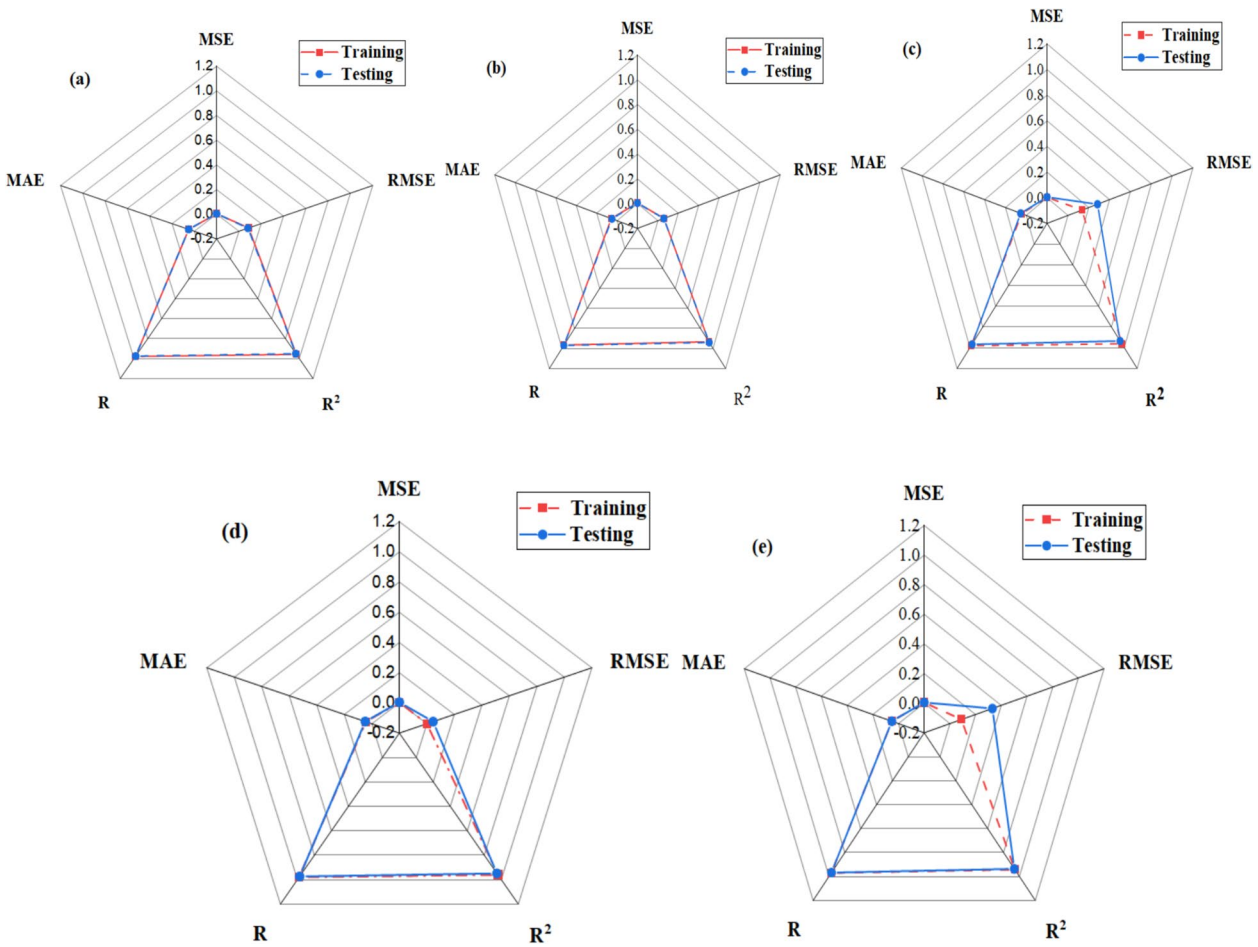

Fig. 19 Evaluation of the performance indicator for **a** ANN, **b** MLR, **c** SVM, **d** GPR, and **e** SWR model

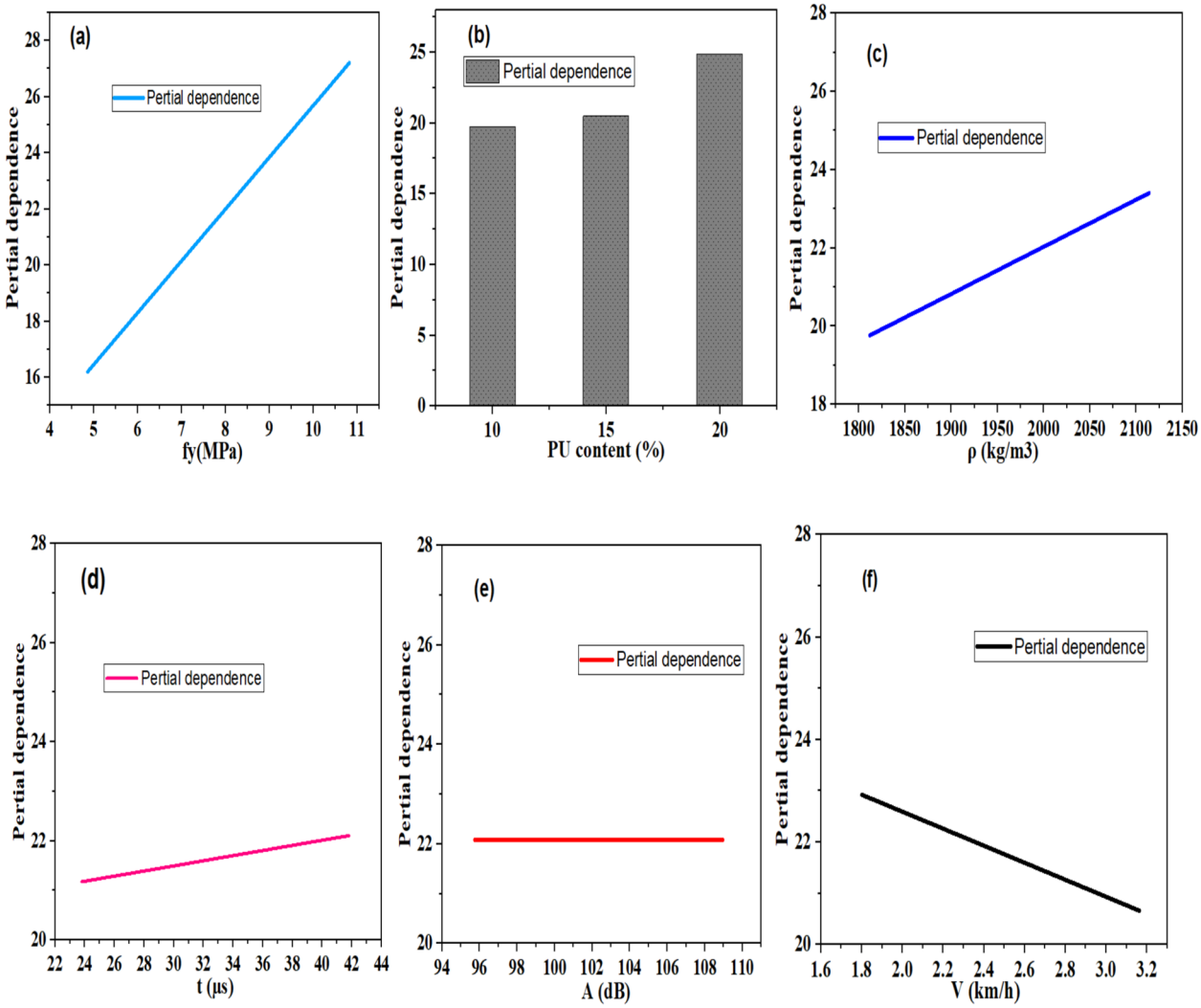

Fig. 20 Partial dependence plots of the ANN model

7 Conclusion

In this study, PUC mixture was developed by mixing aggregate and polyurethane using three mix ratios at 80/20, 85/15, and 90/10 by weight and tested for mechanical and non-destructive tests to obtain experimental datasets for the development of machine learning algorithms to predict the compressive strength. Microstructure analysis was performed on the PUC samples using scanning electron microscopy. The following highlight summarizes the conclusions of this study:

1. The PUC specimens with the better density revealed improved mechanical behavior. The average compressive strength and elastic modulus of the PUC-20 are 99.1% and 125.4% higher than those of PUC-10, respectively. On the other hand, PUC-10 demonstrates the highest UPV value of 3.0494 km/h. The SEM analysis indicates the presence of micro-voids in the PUC-10 microstructure. Conversely, PUC-20 specimens revealed a dense microstructure with the absence crack propagation after testing.
2. The high coefficient correlation values were achieved between the compressive strength and UPV. The feature selection and partial dependence plots showed that the flexural strength is the most relevant and optimal parameter among the input parameters obtained from the mechanical and non-destructive test properties for predicting the compressive. The *t*-test performed between the compressive strength and the potential input parameters revealed that all the parameters are significant.
3. The five developed ML models predicted the PUC's compressive strength with high accuracy. Moreover,

the SVM outperformed other models at the training phase, and the ANN is the best model in the testing phase. Taylor's diagram demonstrates that the standard deviation of all developed models is less than that of the observed data, explaining that the model is not overfitted.

4. The nonlinear models revealed higher estimation accuracy compared to the MLR model due to their robustness in dealing with complex engineering problems. However, all models estimate the strength with higher accuracy, greater than 90%
5. Investigating different parameters obtained from the modified PUC through admixtures such as crumb rubber, milled fiber, and ground glass fiber, and adjusting the hard segment by optimizing PUC's mix formulation is significant. Thus, it is recommended to involve and estimate the overall behavior of the PUC composite considering these ingredients. Moreover, future research should focus on comprehensive non-destructive tests on the PUC to establish its correlation with compressive strength.

Acknowledgements
The authors greatly acknowledge the financial support of this research by the Natural Science Foundation of China (No. 51708314), and the Structures and Materials Laboratory (S&M Lab) of the College of Engineering, Prince Sultan University, Riyadh, Saudi Arabia, for funding the article process fees.

Author contributions
Han Zhu and Yasser E. Ibrahim: conceptualization, investigation, supervision, resources, project administration, funding acquisition: S.I Haruna, and AIB Farouk: conceptualization, methodology, investigation, data curation, writing—original draft, writing—review and editing, visualization. Jianwen shao and Jian Yang: methodology, investigation, writing—review and editing, project, data curation. Musa Adamu and Omar Shabbir Ahmed: writing—review and editing.

Funding
This research is supported by the Natural Science Foundation of China (No. 51708314), and Structures and Materials Laboratory (S&M Lab) of the College of Engineering, Prince Sultan University, Riyadh, Saudi Arabia for funding the article process fees.

Availability of data and materials
The data will be made available only on reasonable request.

Declarations

Competing interests
The authors declared that they had no competing interest.

Received: 6 January 2024 Accepted: 17 May 2025
Published online: 05 August 2025

References

Abba, S. I., Pham, Q. B., Usman, A. G., Linh, N. T. T., Aliyu, D. S., Nguyen, Q., & Bach, Q.-V. (2020). Emerging evolutionary algorithm integrated with kernel principal component analysis for modeling the performance of a water treatment plant. *The Journal of Water Process Engineering (JWPE), 33*, Article 101081. https://doi.org/10.1016/j.jwpe.2019.101081

Adamu, M., Haruna, S. I., Malami, S. I., Ibrahim, M. N., Abba, S. I., & Ibrahim, Y. E. (2021). Prediction of compressive strength of concrete incorporated with jujube seed as partial replacement of coarse aggregate: A feasibility of Hammerstein-Wiener model versus support vector machine. *Modeling Earth Systems and Environment (MESE)*. https://doi.org/10.1007/s40808-021-01301-6

Akber, M. Z. (2024). Improving the experience of machine learning in compressive strength prediction of industrial concrete considering mixing proportions, engineered ratios and atmospheric features. *Construction and Building Materials, 444*, Article 137884. https://doi.org/10.1016/j.conbuildmat.2024.137884

Alas, M., Ali, S. I. A., Abdulhadi, Y., & Abba, S. (2020). I, Experimental evaluation and modeling of polymer nanocomposite modified asphalt binder using ANN and ANFIS. *Journal of Materials in Civil Engineering, 32*, 1–11. https://doi.org/10.1061/(ASCE)MT.1943-5533.0003404

Al-Atroush, M. E., Shabbir, O., Almeshari, B., Waly, M., & Sebaey, T. A. (2021). A novel application of the hydrophobic polyurethane foam: Expansive soil stabilization. *Polymers (Basel)*. https://doi.org/10.3390/polym13081335

Alrayes, F. S., Zakariah, M., Driss, M., & Boulila, W. (2023). Deep neural decision forest (DNDF): A novel approach for enhancing intrusion detection systems in network traffic analysis. *Sensors, 23*, 8362.

Bistričić, L., Baranović, G., Leskovac, M., & Bajsić, E. G. (2010). Hydrogen bonding and mechanical properties of thin films of polyether-based polyurethane–silica nanocomposites. *European Polymer Journal, 46*, 1975–1987. https://doi.org/10.1016/j.eurpolymj.2010.08.001

Carrera, V., Cuadri, A. A., García-Morales, M., & Partal, P. (2015). The development of polyurethane modified bitumen emulsions for cold mix applications. *Materials and Structures, 48*, 3407–3414. https://doi.org/10.1617/s11527-014-0408-2

Chen, C., Seo, H., Jun, C. H., & Zhao, Y. (2022). Pavement crack detection and classification based on fusion feature of LBP and PCA with SVM. *International Journal of Pavement Engineering, 23*, 3274–3283. https://doi.org/10.1080/10298436.2021.1888092

Cong, L., Guo, G., Yang, F., & Ren, M. (2021). The effect of hard segment content of polyurethane on the performances of polyurethane porous mixture. *International Journal of Transportation Science and Technology, 10*, 254–265. https://doi.org/10.1016/j.ijtst.2020.07.003

Cong, L., Yang, F., Guo, G., Ren, M., Shi, J., & Tan, L. (2019). The use of polyurethane for asphalt pavement engineering applications: A state-of-the-art review. *Construction and Building Materials, 225*, 1012–1025. https://doi.org/10.1016/j.conbuildmat.2019.07.213

Diaconescu, R.-M., Barbuta, M., & Harja, M. (2013). Prediction of properties of polymer concrete composite with tire rubber using neural networks. *Materials Science and Engineering B, 178*, 1259–1267. https://doi.org/10.1016/j.mseb.2013.01.014

DL/T5126-2001, Test code on polymer-modified cement martor, National Standard of China, 2001, in: n.d.

Ehsani, M., MoghadasNejad, F., & Hajikarimi, P. (2022). Developing an optimized faulting prediction model in Jointed Plain Concrete Pavement using artificial neural networks and random forest methods. *International Journal of Pavement Engineering*. https://doi.org/10.1080/10298436.2022.2057975

Farouk, A. I. B., & Jinsong, Z. (2022). Prediction of Interface Bond Strength Between Ultra-High-Performance Concrete (UHPC) and Normal Strength Concrete (NSC) Using a Machine Learning Approach. *Arabian Journal for Science and Engineering*. https://doi.org/10.1007/s13369-021-06433-6

Gad, M. A., Nikbakht, E., & Ragab, M. G. (2024). Predicting the compressive strength of engineered geopolymer composites using automated machine learning. *Construction and Building Materials, 442*, Article 137509. https://doi.org/10.1016/j.conbuildmat.2024.137509

Gallu, R., Méchin, F., Dalmas, F., Gérard, J.-F., Perrin, R., & Loup, F. (2020). Rheology-morphology relationships of new polymer-modified bitumen based on thermoplastic polyurethanes (TPU). *Construction and Building Materials, 259*, Article 120404. https://doi.org/10.1016/j.conbuildmat.2020.120404

Gao, H., & Sun, Q. (2020). Study on fatigue test and life prediction of polyurethane cement composite (PUC) under high or low temperature conditions. *Advances in Materials Science and Engineering, 2020*, 2398064. https://doi.org/10.1155/2020/2398064

Garbacz, A. & Garboczi, E.J. (2003). Ultrasonic evaluation methods applicable to polymer concrete composites, US Department of Commerce, National Institute of Standards and Technology.

Ghassemi, P., & Toufigh, V. (2020). Durability of epoxy polymer and ordinary cement concrete in aggressive environments. *Construction and Building Materials, 234*, Article 117887. https://doi.org/10.1016/j.conbuildmat.2019.117887

Ghosh, R., Sagar, S. P., Kumar, A., Gupta, S. K., & Kumar, S. (2018). Estimation of geopolymer concrete strength from ultrasonic pulse velocity (UPV) using high power pulser. *The Journal of Building Engineering (JOBE), 16*, 39–44. https://doi.org/10.1016/j.jobe.2017.12.009

Haruna, S. I., Bashir, A., Abba, S. I., Ibrahim, Y. E., Gomma, S., Gora, A. M., & Nawar, M. T. (2025b). Metaheuristic-based prediction of shear resistance of headed stud connectors embedded in concrete coupled with SHAP explainability. *Results in Engineering, 25*, Article 104445. https://doi.org/10.1016/j.rineng.2025.104445

Haruna, S. I., Ibrahim, Y. E., & Umar, I. K. (2025a). Machine Learning Approach for Prediction and Reliability Analysis of Failure Strength of U-Shaped Concrete Samples Joined with UHPC and PUC Composites. *J. Compos. Sci.* https://doi.org/10.3390/jcs9010023

Haruna, S. I., Malami, S. I., Adamu, M., Usman, A. G., Farouk, A. I. B., Ali, S. I. A., & Abba, S. I. (2021). Compressive strength of self-compacting concrete modified with rice husk ash and calcium carbide waste modeling: A Feasibility of emerging emotional intelligent model (EANN) versus traditional FFNN. *Arabian Journal for Science and Engineering, 46*, 11207–11222. https://doi.org/10.1007/s13369-021-05715-3

Haruna, S. I., Zhu, H., Ibrahim, Y. E., Shao, J., Adamu, M., & Farouk, A. I. B. (2022). Experimental and Statistical Analysis of U-Shaped Polyurethane-Based Polymer Concrete under Static and Impact Loads as a Repair Material. *Buildings, 12*, 1986.

Hastie, T., Tibshirani, R., Friedman, J. H., & Friedman, J. H. (2009). *The elements of statistical learning: data mining, inference, and prediction*. Springer.

Hoang, N.-D., Pham, A.-D., Nguyen, Q.-L., & Pham, Q.-N. (2016). Estimating compressive strength of high performance concrete with Gaussian process regression model. *Advances in Civil Engineering, 2016*, 2861380. https://doi.org/10.1155/2016/2861380

Hoang, N.-D., Tran, X.-L., & Nguyen, H. (2020). Predicting ultimate bond strength of corroded reinforcement and surrounding concrete using a metaheuristic optimized least squares support vector regression model. *Neural Computing and Applications, 32*, 7289–7309.

Huang, H., Pang, H., Huang, J., Yu, P., Li, J., Lu, M., & Liao, B. (2021). Influence of hard segment content and soft segment length on the microphase structure and mechanical performance of polyurethane-based polymer concrete. *Construction and Building Materials, 284*, Article 122388. https://doi.org/10.1016/j.conbuildmat.2021.122388

Huang, H., Pang, H., Huang, J., Zhao, H., & Liao, B. (2020a). Synthesis and characterization of ground glass fiber reinforced polyurethane-based polymer concrete as a cementitious runway repair material. *Construction and Building Materials*. https://doi.org/10.1016/j.conbuildmat.2019.117221

Huang, H., Pang, H., Huang, J., Zhao, H., & Liao, B. (2020b). Synthesis and characterization of ground glass fiber reinforced polyurethane-based polymer concrete as a cementitious runway repair material. *Construction and Building Materials, 242*, Article 117221. https://doi.org/10.1016/j.conbuildmat.2019.117221

Ibrahim Haruna, S., Zhu, H., Jiang, W., & Shao, J. (2021). Evaluation of impact resistance properties of polyurethane-based polymer concrete for the repair of runway subjected to repeated drop-weight impact test. *Construction and Building Materials, 309*, 125152. https://doi.org/10.1016/j.conbuildmat.2021.125152

Javid, A., & Toufigh, V. (2024). Utilizing ensemble machine learning and gray wolf optimization to predict the compressive strength of silica fume mixtures. *Structural Concrete, 25*, 4048–4074. https://doi.org/10.1002/suco.202301135

Jia, M., Sha, A., Lin, J., Zhang, Z., Qi, B., & Yuan, D. (2021). Polyurethane asphalt binder: A promising candidate for steel bridge deck-paving material. *International Journal of Pavement Engineering*. https://doi.org/10.1080/10298436.2021.1927028

Jiang, W., Zhu, H., Haruna, S. I., Zhao, B., Shao, J., & Yu, Y. (2021). Effect of crumb rubber powder on mechanical properties and pore structure of polyurethane-based polymer mortar for repair. *Construction and Building Materials, 309*, Article 125169. https://doi.org/10.1016/j.conbuildmat.2021.125169

Jiang, W., Zhu, H., Ibrahim Haruna, S., Shao, J., Yu, Y., & Wu, K. (2022b). Mechanical properties and freeze–thaw resistance of polyurethane-based polymer mortar with crumb rubber powder. *Construction and Building Materials, 352*, Article 129040. https://doi.org/10.1016/j.conbuildmat.2022.129040

Jiang, Z., Tang, C., Yang, J., You, Y., & Lv, Z. (2022a). A lab study to develop polyurethane concrete for bridge deck pavement. *International Journal of Pavement Engineering, 23*, 1404–1412. https://doi.org/10.1080/10298436.2020.1804063

Junaedi, H., Khan, T., & Sebaey, T. A. (2023). Characteristics of Carbon-Fiber-Reinforced Polymer Face Sheet and Glass-Fiber-Reinforced Rigid Polyurethane Foam Sandwich Structures under Flexural and Compression Tests. *Materials (Basel)*. https://doi.org/10.3390/ma16145101

Jung, K.-C., Roh, I.-T., & Chang, S.-H. (2014). Evaluation of mechanical properties of polymer concretes for the rapid repair of runways. *Composites Part B: Engineering, 58*, 352–360. https://doi.org/10.1016/j.compositesb.2013.10.076

Kooshkaki, A., & Eskandari-Naddaf, H. (2019). Effect of porosity on predicting compressive and flexural strength of cement mortar containing micro and nano-silica by multi-objective ANN modeling. *Construction and Building Materials, 212*, 176–191. https://doi.org/10.1016/j.conbuildmat.2019.03.243

Kumar, P., Nigam, S. P., & Kumar, N. (2014). Vehicular traffic noise modeling using artificial neural network approach. *Transportation Research Part C: Emerging Technologies, 40*, 111–122. https://doi.org/10.1016/j.trc.2014.01.006

Li, S.-X. & Liu, Y.J. (2002). Polyurethane resin and its application.

Long, X., Lu, C., Su, Y., & Dai, Y. (2023a). Machine learning framework for predicting the low cycle fatigue life of lead-free solders. *Engineering Failure Analysis, 148*, Article 107228. https://doi.org/10.1016/j.engfailanal.2023.107228

Long, X., Mao, M., Su, T., Su, Y., & Tian, M. (2023b). Machine learning method to predict dynamic compressive response of concrete-like material at high strain rates. *Defence Technology, 23*, 100–111. https://doi.org/10.1016/j.dt.2022.02.003

Marinela, B., Rodica-Mariana, D., & Maria, H. (2012). Using neural networks for prediction of properties of polymer concrete with fly ash. *Journal of Materials in Civil Engineering, 24*, 523–528. https://doi.org/10.1061/(ASCE)MT.1943-5533.0000413

Nourani, V., & Sharghi, Z. A. E. (2020). Sensitivity analysis and ensemble artificial intelligence-based model for short-term prediction ofNO 2 concentration. *International Journal of Environmental Science and Technology*. https://doi.org/10.1007/s13762-020-03002-6

Omran, B. A., Chen, Q., & Jin, R. (2016). Comparison of data mining techniques for predicting compressive strength of environmentally friendly concrete. *Journal of Computing in Civil Engineering, 30*, 4016029.

Pal, M., & Deswal, S. (2010). Modelling pile capacity using Gaussian process regression. *Computers and Geotechnics, 37*, 942–947.

Peng, H., Long, F., & Ding, C. (2005). Feature selection based on mutual information criteria of max-dependency, max-relevance, and min-redundancy. *IEEE Transactions on Pattern Analysis and Machine Intelligence, 27*, 1226–1238.

Shao, J., Zhu, H., Zuo, X., Lei, W., Borito, S. M., Liang, J., & Duan, F. (2020). Effect of waste rubber particles on the mechanical performance and deformation properties of epoxy concrete for repair. *Construction and Building Materials, 241*, Article 118008. https://doi.org/10.1016/j.conbuildmat.2020.118008

Somarathna, H. M. C. C., Raman, S. N., Mohotti, D., Mutalib, A. A., & Badri, K. H. (2018). The use of polyurethane for structural and infrastructural engineering applications: A state-of-the-art review. *Construction and Building Materials, 190*, 995–1014. https://doi.org/10.1016/j.conbuildmat.2018.09.166

Song, H., Ahmad, A., Farooq, F., Ostrowski, K. A., Maślak, M., Czarnecki, S., & Aslam, F. (2021). Predicting the compressive strength of concrete with fly ash admixture using machine learning algorithms. *Construction and Building Materials, 308*, Article 125021. https://doi.org/10.1016/j.conbuildmat.2021.125021

Sun, M., Zheng, M., Qu, G., Yuan, K., Bi, Y., & Wang, J. (2018). Performance of polyurethane modified asphalt and its mixtures. *Construction and Building*

Materials, 191, 386–397. https://doi.org/10.1016/j.conbuildmat.2018.10.025
Taylor, K. E. (2001). Summarizing multiple aspects of model performance in a single diagram. *Journal of Geophysical Research, 106*, 7183–7192. https://doi.org/10.1029/2000JD900719
Thakur, M. S., Pandhiani, S. M., Kashyap, V., Upadhya, A., & Sihag, P. (2021). Predicting bond strength of FRP bars in concrete using soft computing techniques. *Arabian Journal for Science and Engineering, 46*, 4951–4969.
Umar, I. K., Nourani, V., & Gokcekus, H. (2021). A novel multi-model data-driven ensemble approach for the prediction of particulate matter concentration. *Environmental Science and Pollution Research, 28*, 49663–49677.
Vasconcelos, P. V., Lino, F. J., Magalhães, A., & Neto, R. J. L. (2005). Impact fracture study of epoxy-based composites with aluminium particles and milled fibres. *Journal of Materials Processing Technology, 170*, 277–283. https://doi.org/10.1016/j.jmatprotec.2005.05.006
Wang, Y., Sun, Q., Ding, H., Jia, D., & Li, C. (2021). Effect of binder-aggregate ratio on the mechanical and functional properties of porous polyurethane cement mixture. *International Journal of Pavement Engineering*. https://doi.org/10.1080/10298436.2021.1995734
Williams, C. K., & Rasmussen, C. E. (2006). *Gaussian processes for machine learning*. MIT press Cambridge.
Wu, X., Dong, Y., Zhang, Y., & Liu, J. (2020). River runoff influence factors recognition using stepwise regression analysis: The case of a northern Chinese coal mining Area. *Polish Journal of Environmental Studies, 29*, 893–900. https://doi.org/10.15244/pjoes/103360
Yang, S., Sun, J., & Zhifeng, X. (2024). Prediction on compressive strength of recycled aggregate self-compacting concrete by machine learning method. *The Journal of Building Engineering (JOBE), 88*, Article 109055. https://doi.org/10.1016/j.jobe.2024.109055
Yasar, A., Bilgili, M., & Simsek, E. (2012). Water demand forecasting based on stepwise multiple nonlinear regression analysis. *Arabian Journal for Science and Engineering, 37*, 2333–2341. https://doi.org/10.1007/s13369-012-0309-z
Yaseen, Z. M., Deo, R. C., Hilal, A., Abd, A. M., Bueno, L. C., Salcedo-Sanz, S., & Nehdi, M. L. (2018). Predicting compressive strength of lightweight foamed concrete using extreme learning machine model. *Advances in Engineering Software, 115*, 112–125. https://doi.org/10.1016/j.advengsoft.2017.09.004

Publisher's Note

S. I. Haruna PhD, Postdoc researcher in Engineering Management Department, College of Engineering, Prince Sultan University, Riyadh 11586, Saudi Arabia.

Han Zhu PhD, Professor in School of Civil Engineering, Tianjin University, Tianjin 300350, China.

Yasser E. Ibrahim PhD, Professor in Engineering Management Department, College of Engineering, Prince Sultan University, Riyadh 11586, Saudi Arabia.

Jian Yang Postgraduate Student, School of Civil Engineering, Tianjin University, Tianjin 300350, China.

AIB Farouk PhD, Postdoc researcher in Interdisciplinary Research Center for Construction and Building Materials, King Fahd University of Petroleum and Minerals, Dhahran 31261, Saudi Arabia.

Jianwen Shao PhD, Assistance Professor in School of Civil Engineering, Ludong University, Yantai 264025, China.

Musa Adamu Researcher in Engineering Management Department, College of Engineering, Prince Sultan University, Riyadh 11586, Saudi Arabia.

Omar Shabbir Ahmed Masters, Research Engineerin Engineering Management Department, College of Engineering, Prince Sultan University, Riyadh 11586, Saudi Arabia.